Evidence for undamped waves on ohmic materials

Tese apresentada ao programa de Pós-Graduação do Departamento de Física do Instituto de Ciências Exatas da Universidade Federal de Minas Gerais como requisito parcial à obtenção to grau de Doutor em Ciências.

Roberto Batista Sardenberg

Orientador: Prof. Dr. José Marcos Andrade Figueiredo

Página intencionalmente deixada em branco para a inserção da folha de aprovação.

Agradecimentos

Primeiramente agradeço ao meu orientador, prof. Dr. José Marcos Andrade Figueiredo. Agradeço por sua incansável atenção. É notável a sua dedicação ao conhecimento, sem a qual, a realização desse trabalho não seria possível.

Agradeço também a minha esposa Sâmua que sempre me apoiou em todos os meus projetos pessoais com carinho e dedicação.

Agradeço a todos os funcionários do Departamento de Física, em especial a bibliotecária Shirley que, sendo um poço de eficiência, sempre atendeu de prontidão as demandas bibliográficas deste trabalho.

Agradeço ao professor Dr. Klaus Krambrock que disponibilizou prontamente alguns recursos do laboratório sob sua supervisão, e que foram muito úteis na realização desse trabalho.

Agradeço ainda as agências CNPq, CAPES e FAPEMIG pelo apoio que prestam ao desenvolvimento de pesquisas na Universidade Federal de Minas Gerais.

Contents:

Abstract

We present in this work a yet unexploited property of the Maxwell equations when applied to conductors. It was found that the real part impedance of passive circuits can achieve negative values. We have performed calculations which forecast this so far unobserved part of the impedance spectrum of conducting materials. A series of experiments which confirms our predictions was also conducted. The impedance of single spires and also of some coils of specific geometry were measured in the MHz frequency range. Metallic and carbon wires were used in constructing these spires and coils. Spectral analyses of our data demonstrate that in fact, the impedance of these passive circuits presents a frequency-dependent phase angle able to cover the full trigonometric cycle $[-\pi, \pi]$.

Besides direct impedance readings, additional experiments were performed in order to check our data against possible systematic errors. We have constructed and enclosed our circuits within several kinds of electromagnetic shields, all of them presenting wall thickness several times larger than the skin dept of the radiation in the frequency range of measurement. With this, we guaranteed that external sources could not possibly induce any relevant noise in our measurements. The negative real part impedance effects were also present on these shielded experiments. In addition to that, it was confirmed on an oscilloscope screen that the voltage and current on a passive circuit may, in fact, present a phase difference of π.

A first-principles theoretical model that assumes the presence of longitudinal undamped waves propagating in the system was devised. An expression for the impedance of circuits possessing theses waves was then obtained. This way we were able to make numerical calculations and predict the negative real part impedance effects. Experimental evidence for the existence of these longitudinal waves was also obtained. On these footings we have pointed out a special propagation mode of the electromagnetic field as the cause of the unusual observed spectral response. A discussion on the validity of impedance data and causality issues is also presented.

1-Introduction

Impedance measurements are one of the most used techniques available to study material properties as well as electromagnetic devices and circuits. This way, novelties on device construction and circuit technology associated to new material properties and/or unusual field dynamics generally rely on results supported by impedance data.

The variety of material properties relevant to the interaction of electromagnetic fields with matter led to the development of passive circuit elements and active devices designed to control charges and currents in matter. This allows the advent of technologies inherent to almost all aspects of modern human life. Passive circuit elements are based on equations relating field and matter variables, as defined by the constitutive relations, and are crucial in determining the best performance and economic viability of practical circuits. In this case, a property of Maxwell equations which has not yet been considered could determine new relations between fields and currents, thus allowing new circuit configurations or even new circuit elements.

In this work we present a so far concealed part of the impedance spectrum of passive circuits. We have found that the real part of the impedance of carefully designed passive devices may attain negative values in a specific frequency range of measurement. Both field theoretical calculations and a set of experiments were performed. The systems studied comprise single spires and also coils which were constructed with metallic and carbon wires, possessing different geometries. Calculated and measured data are in good agreement and display the negative impedance effects.

Due to the inherent dissipative character of the ohmic regime, it is expected that the real part of the impedance increases as the frequency of the applied excitation signal becomes larger. It is known that this effect is caused by magnetic forces inside the material, which push charge carriers to the longitudinal surface of the material in such a way that the effective transversal area available to charge transport becomes smaller than the geometric one - the skin effect. However, for longer wires we have observed that this effect is lessened, being almost minimal. Our data show that, as frequency increases the real part of the impedance gets a maximum. Further increases in frequency lead to smaller values of the real part, which may even assume negative values. This is an effect that field dynamics relevant to skin calculations cannot account for.

For still larger frequencies a kind of abnormal resonance peak, in the sense that it is inverted when compared to usual RLC peaks, is observed. This means that the spire presents a 'negative resistance' component forming its impedance spectral response. As a consequence, the observed resonances admit an extended phase angle variation, ranging from $-\pi$ to π instead of the usual $-\pi/2$ to $\pi/2$ interval, defined in its limits by the reactance of pure capacitances and inductances.

1.1-Organization of the work

We first expose a brief historical background of impedance spectroscopy technique, pointing out the foundations as well as referencing later developments and recent advances.

Following, in Chapter 2, we present the concept of impedance of a linear system. We then define, more specifically, how electrical impedance measurements are made. The most used method for electrical impedance measurement is described in detail. In sequence, the theoretical formalism of electromagnetism is reviewed. The set of Maxwell equations are presented and the formulation of potentials is shown. Besides that, some fundamental electromagnetic effects and usual impedance calculations are derived. These effects are thoroughly disseminated in the literature and provide the basis for the understanding of several devices which comprise the basic circuit elements of electronics.

In Chapter 3 we present a first-principle theoretical model which assumes the presence of undamped longitudinal current waves along the length of a conducting material. This assumption was never made, to the best of our knowledge, to the kind of systems and frequency range that was used in this work. By use of the Maxwell-Faraday equation and the retarded vector potential in the Lorentz gauge, we were able to generate an impedance formula and perform numerical calculations. These calculations predicted the negative real part impedance effect which was confirmed by a sequence of carefully executed experiments.

In sequence, we present in Chapter 4 a detailed description of the performed experiments, confirming our predictions. First, we show experimental evidence for the presence of these current waves along the wire length of a conductor, justifying the assumptions made in our model. In sequence, direct impedance measurement data for several circuits are displayed. The impedance spectra of single spires and coils of

different lengths and wire materials are displayed. These spectra present the negative real part impedance which was predicted by our theoretical model. A major concern when performing our experiments was the possibility that the measured negative real part impedances were due to the interference of external electromagnetic sources. In order to check if that was the case, we have constructed several kinds of electromagnetic shields to enclose our circuits. All of the shields were constructed with metallic walls several times thicker than the skin dept of the radiation in the measurement frequency range. All of the resulting impedance spectra for the shielded experiments still presented negative real part impedance effects. Besides that, additional experimental evidence such as the linearity of the measurements proves that no external sources could be responsible for the observed phenomenon. On an oscilloscope screen it was also possible to confirm that the voltage and current of a passive circuit can achieve a phase angle of π.

In Chapter 5 we provide a discussion on the validity of impedance data. Linear System Theory provides the grounds for impedance spectroscopy technique and imposes some constrains that must be satisfied by any physically realizable impedance. In particular, Linear System Theory demands that the impedance must be a causal function. A causal impedance function is a guarantee that no effect will precede its cause. In a loose manner, inside an electrical circuit it means that no current will rise before the potential difference is applied. It will be shown that the impedance will only be a causal function if its real and imaginary parts are not independent of each other but constitute a Hilbert transform pair instead. It will be also shown in Chapter 5 that the impedance formula we have derived by assuming longitudinal waves naturally satisfies this causality condition.

Finally, in Chapter 6 we present our concluding arguments and perspectives.

1.2-Historical background

Due to the immediate applicability of almost all electromagnetic phenomena, materials containing non-trivial electronic properties are highly sought-after. To this end, there has recently been a marked search for new materials or special molecular arrangements in the nanoscale domain, featuring better device performance, low fabrication cost and/or low energy consumption [1-2]. On more general grounds, Strukov, Snider, Stewart and Williams [3] recently found the menristor, the last circuit element that can be derived from the fundamental relations of circuit variables, which

was predicted by Chua [4]. Therefore, any novelty in circuit configuration or circuit size, such as the use of quantum dynamics in practical devices [5-7] or new materials [8-11] can enhance their applicability. Likewise, the discovery of a new field dynamics in matter would also be of relevance in determining the properties of existing circuit elements or even lead to the development of new ones.

The grounds for impedance spectroscopy were introduced by Heaviside in the late nineteenth century with the advent of the Linear System Theory. Warburg then extended the concept to electrochemical systems and derived the impedance for a system undergoing a diffusion process [12]. A few decades later, at the middle of the twentieth century, the potentiostat was invented. Nevertheless, it was only after the 1970's, with the invention of the frequency response analyzers, that this technique become widely used. In fact, a wide set of distinct phenomena was studied with the aid of impedance spectroscopy.

The field of electrochemistry has greatly benefitted from impedance spectroscopy. In particular, the task of elucidating and characterizing corrosion mechanisms was only achieved due to the application of this technique [13]. As very useful in determining the electrical response of devices, impedance spectroscopy has also been used to characterize and design continuously better circuit components [14-16].

Several attempts to improve this technique and extend its limits of applicability have been carried out. Self-calibration methods [17-18] and digital signal-processing solutions [19] are examples of an effort to minimize impedance errors. Also a great amount of survey was dedicated to augment the frequency range of measurement. A common limiting factor at high frequency values is the signal loss due to cabling impedances. The impedance of cables at high frequencies can be measured by the Time Domain Reflectometry technique [20]. Also at high frequency values, the impedance spectroscopy can be useful in determining electromagnetic response of antennas [21-23], which is a cornerstone for communications [24]. Nowadays the electrical impedance of a system can be measured at very low (~μHz), as well as very high frequencies (microwave and mm-waves) [25-28]. However there is a window in that broad frequency range that has been proven difficult to work with (dozens of MHz to thousands of MHz). Apparently the metrology for this specific frequency range has presented several challenges in producing good standards of impedance and generating proper calibration for instruments [29]. Other phenomena also studied with the aid of

impedance spectroscopy range from electronic conduction in polymers [30] and ionic mobility of nanostructures [31] to biophysics applications such as the study of cell migration [32] and toxicology [33]. This technique has also been efficient in the determination of state-of-charge and state-of-health of batteries [34]. Impedance measurements are also available in the context of microscopic techniques at the microwave frequency range. In this case, one can retrieve a map of resistance and capacitance of a microscopic sample [35].

Given the wide range of applicability, and the possibility of retrieving valuable physical information such as those concerning transport, dielectric relaxation and corrosion phenomena, it is clear that any advance towards improving the impedance technique is certainly much welcome.

Negative real part impedances have been reported on the context of electrochemical impedance spectroscopy [36-38] and on quantum systems under the presence of microwave radiation [39]. Besides, specific devices possessing negative resistance and negative differential resistance are of widespread usage on electronics, as for example; Tunnel diodes, Gunn diodes, gas discharge tubes and thyristors. All of the examples cited above are fed by an external source of energy, whereas electrochemical systems may present active electrode reactions, which could drive energy into the circuit. So they cannot be considered as passive devices. The seminal work of Bode [40] gave us the basis of circuit theory for negative resistances, although he only considers this possibility on active circuits.

A more subtle point that is not clear on the literature at the present moment is the possibility of a passive circuit to present negative real part impedance. At first thought, it might seem that a passive circuit could not present negative resistance effects, but we show in this work, that this is not the case.

2-Impedance definition, measurement and calculations

In this chapter we first provide a definition for the impedance of a linear system. Then, in a more specific way, the electrical impedance is discussed. In sequence, we expose a method of measurement that is usually employed by commercial impedance meters. We also present a brief review on the classical formulation of electromagnetism by presenting the set of Maxwell equations and by making use of the electromagnetic potentials. Guidelines to the general solution of the non-homogeneous wave equation are also given. Several phenomena which are conspicuous and define the impedances of common usage on electrical devices are then considered. The impedances of the classical circuit elements which constitute a basis for electronics are derived.

2.1-The concept of impedance of a linear system

The impedance of a linear system is defined as the ratio between some externally applied excitation and the resulting response. This excitation may have different forms including electrical, optical or mechanical oscillations. In the case of acoustic impedance for example, the excitation signal may be a pressure wave generated by a controlled explosion while the measured response may be a mechanical vibration of the soil. Thus, the concept of impedance is defined in order to quantify the ability of a system to react to some external stimulus. Figure 1 below illustrates in a schematic way this relationship:

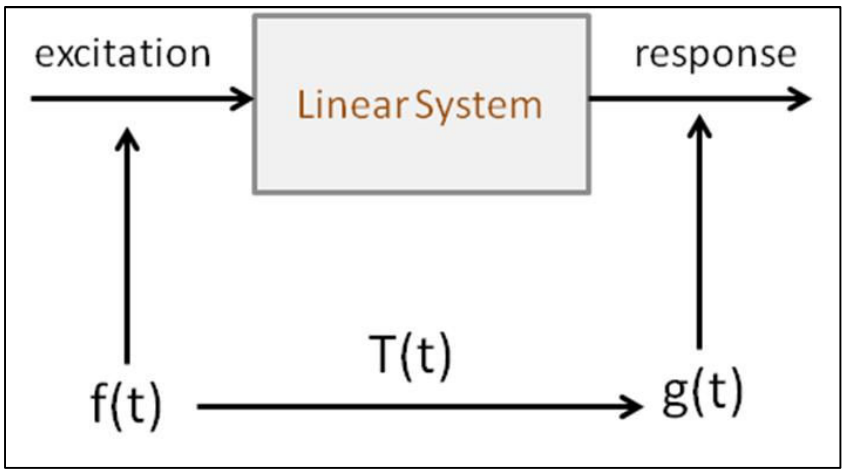

Figure 1: Schematic illustration of relationship between excitation and response of a linear system.

On Figure 1, the time dependent applied excitation is represented by the function f(t) and the resulting response by the function g(t). As consequence of Linear System Theory (which is discussed with more detail on Chapter 5), there must exist a causal Transfer function T(t) which connects the cause (excitation), to the response of the system. In a general way, the input may be written as a convolution of the transfer function with the output of the system as given below:

$$f(t) = \int_{-\infty}^{\infty} T(u-t)g(u)du \quad \Rightarrow \quad F(\omega) = Z(\omega)G(\omega) \tag{1}$$

Equation 1 provides a general definition of the impedance (Z=stimulus/response) of a linear system. The Convolution Theorem and Fourier representation were applied in order to define the impedance of the system in the frequency instead of time domain.

The impedance of non-linear systems may also be defined and measured [41] as well. However, the problem of treating non-linear impedances is somewhat more involved because the response may be a function of the excitation input itself. Only linear systems are considered in this work.

2.2-Definition of electrical impedance

The electrical impedance of a system is obtained by first submitting the sample under study to an alternating potential difference, and then by measuring the resulting electrical current. Generally, this applied signal is sinusoidal, and the frequency of oscillation is varied within an interval which is as broad as possible in order to obtain a maximum amount of information. Two physical parameters are measured. One of them is the ratio between the amplitudes of the applied potential and the resulting current. The other is the phase difference between the applied voltage and the current in the sample. These two parameters, seen as functions of the applied frequency, carry the electrical response information of the system under study. In order to define electrical impedance in a precise way, suppose that a sinusoidal signal $V(\omega,t)$ is applied across two points of a sample. We may write this excitation potential, using the complex signals notation [42] as:

$$V(\omega,t) = V_o e^{i\omega t} \tag{2}$$

The actual applied potential difference is given by the real part of Equation 2. Then a current will rise in response to this excitation and, if the sample is a linear and passive material, we can write it as:

$$I(\omega,t) = I_o(\omega)e^{i[\omega t - \phi(\omega)]} \tag{3}$$

The same complex signals notation of Equation 2 was used here, that is, the current in the sample is given by the real part of Equation 3. By introducing this notation, the definition of impedance and several other calculations are made easier. The electrical impedance is then defined as the ratio of the excitation signal to the response current in the sample:

$$Z(\omega) \equiv \frac{V(\omega,t)}{I(\omega,t)} = \frac{V_o}{I_o(\omega)}e^{i\phi(\omega)} \tag{4}$$

The impedance is then defined as a complex valued function of the applied frequency. Its modulus is retrieved by calculating the ratio of the excitation and response amplitudes and the phase angle is obtained from the direct measurement of the phase difference of the applied signal and the resulting current. The impedance modulus and phase angle (or equivalently, the real and imaginary parts) are usually given as function of the applied frequency in the form of a spectrum.

Notice that, for a time-invariant system, the time dependence is canceled out in Equation 4, leaving a stable impedance function. This means that the impedance as defined by that equation only makes physical sense if the system does not evolve with time, that is, it is at a stationary state due to the continuously applied excitation. In fact, the impedance function must satisfy some quite general criteria imposed by Linear System Theory (LST) in order to represent real systems. These criteria are discussed in detail on Chapter 5. The necessity of a steady state system means that, in practice, a time interval between the starting of the excitation and the response current measuring must be kept in order to permit all transients due to the buildup of electromagnetic fields inside the sample to vanish. This fact presents no constrains in the measurements of highly conducting materials such as metals. This is because the dielectric relaxation times for these materials are very low. The reciprocals of these characteristic times are much higher than the typical frequencies in an impedance experiment, and would only be relevant near the optical regime.

2.3-The usual method for impedance measurements

There are several means of measuring the impedance of a device, as for example, by making it balance a bridge or by using the unknown impedance on a resonant circuit [43]. For every frequency range or desired application, a different measurement method proves to be the best in providing reliable impedance results. For the range of MHz the most wide spread method is based on the direct measurement of the applied voltage and resulting current in the sample, which is also converted on a voltage. This procedure is commonly employed by commercial impedancemeters and has the advantage of being easily automated, generating easy to use equipments. Further details of this widespread method are described below.

2.3.1-Impedance modulus measurement

In order to obtain the impedance modulus of a device under test (DUT), a known potential difference is applied to this device, and the resulting current is converted into another potential difference by a wide frequency range impedance converter. This procedure is schematized below on Figure 2:

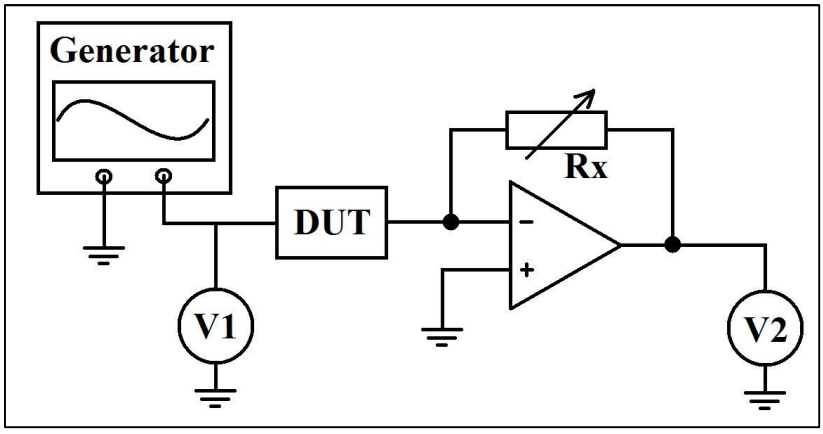

Figure 2: Principles of impedance modulus measuring method.

As shown on Figure 2, the AC voltage from the generator is applied to the sample and measured as V1. The DUT current (I), feeds an operational amplifier with an inverting input, which has the variable resistor Rx in its feedback loop. A value of Rx is chosen so that the output voltage V2 of the operational amplifier is in a good measurable range. Then the voltage V2 is related to the DUT current as $I = -V2/Rx$, if

the operational amplifier is considered to be ideal (virtual ground with zero input impedance at the current input). The voltage V1 is the potential difference across the device. With these considerations, DUT impedance modulus is obtained from:

$$Z_{DUT} = \frac{V1}{I} = \frac{-V1}{V2} Rx$$

The measurement of voltages V1 and V2 are actually phase sensitive. That is necessary in order to obtain the DUT impedance phase angle. The method usually employed to obtain the difference of phases of those signals is explained in sequence.

2.3.2-Impedance phase angle measurement

As already shown on Figure 2, the signal from an AC generator is applied to a DUT. In order to obtain the phase difference introduced by the DUT, two signal correlators are used. This is illustrated on Figure 3 below, which shows the signal arising from the DUT. It is displaced by a phase angle ϕ in relation to the generator. This signal is multiplied by the signal of the generator itself and integrated on the temporal parameter along an integer number N of periods. The result of this operation is a DC voltage which is proportional to cos(ϕ).

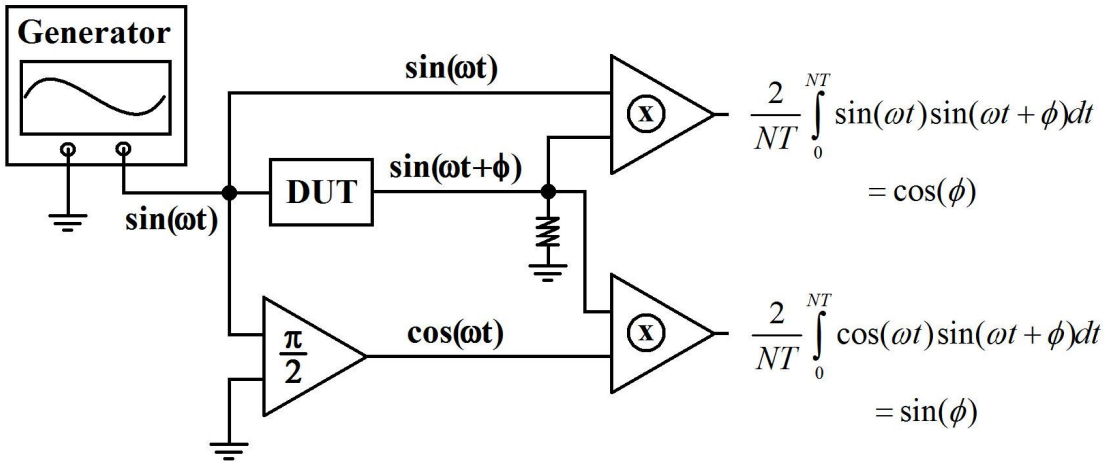

Figure 3: Principles of impedance phase angle measuring method. The element with a symbol π/2 has the function of shifting the signal by a phase angle of π/2. The elements with the circled x symbols have the function of multiplying and integrating the signals. Their operation is represented by the equations also shown on this figure.

Also, another portion of the signal is drawn from the generator and displaced by an angle of π/2. The signal arising from the DUT is also multiplied by this second displaced signal and integrated in another correlator. After integration, a DC voltage which is proportional to sin(ϕ) is obtained. This way, the phase angle defined on Equation 4 is measured.

2.4-Basic laws of electromagnetism and theoretical formalism

In this section we present the basic theoretical formalism by presenting the set of Maxwell equations as well as by defining the gauge transformations and electromagnetic potentials. The steps to obtaining the general solution of the inhomogeneous wave equations are provided, and the concept of retarded potentials naturally arises from these guidelines.

2.4.1-Maxwell equations

Generally, the starting point of impedance calculations is the set of Maxwell equations. That is because they are the basic governing laws for the whole discipline of electromagnetism. This set of partial differential equations is summarized below:

$$\vec{\nabla}.\vec{E} = \frac{\rho}{\varepsilon_o} \qquad \text{Gauss's Law}$$

$$\vec{\nabla}.\vec{B} = 0 \qquad \text{Gauss's Law of Magnetism}$$

$$\vec{\nabla} x \vec{E} = -\frac{\partial \vec{B}}{\partial t} \qquad \text{Faraday's Law}$$

$$\vec{\nabla} x \vec{B} = \mu_o \vec{J} + \frac{1}{c^2}\frac{\partial \vec{E}}{\partial t} \qquad \text{Ampère-Maxwell Law}$$

These equations, as written above, are valid for the case of the presence of sources in free space. By sources we mean an electrical charge densities (ρ) and/or current densities ($\vec{J}$). The constant $\varepsilon_o = 8.85x10^{-12} F/m$ is called the electrical permittivity, the constant $\mu_o = 4\pi x10^{-7} H/m$ the magnetic permeability of the free space and the speed of light c has the following definition: $c = 1/\sqrt{\mu_o \varepsilon_o}$.

A generalization to the less restrictive case of a linear isotropic media is made by replacing the vacuum constants by the constants of a particular material: $\varepsilon_o \to \varepsilon$, $\mu_o \to \mu$ and $c \to v = 1/\sqrt{\mu\varepsilon}$. Inside the material, these physical properties can actually be frequency dependent. Also, it may be useful to define constitutive relations and auxiliary fields such as the electric displacement, in order to consider the presence of polarizations and magnetizations which could be built inside the media. These auxiliary fields are the macroscopic average from the spatial and temporal abrupt changing microscopic fields of the individual constituents. The more general case of a non-isotropic media requires the introduction of tensorial equations. Besides that, there is also a possibility that, for some material, non-linearities are present, in such a way that the permeability and permittivity are not simple constants, but functions of the fields themselves.

For the kind of problems we intent to treat in this work it will not be necessary to define those auxiliary fields, nor to consider frequency or space dependent material properties. It will suffice to consider the free space case which is ruled by the set of differential equations just given above. That is because in our case the electromagnetic fields will extend themselves into linear isotropic media only. For example, a case of interest will be that of a single spire constructed with a thin metallic wire, in the open air. In this case, almost all of the fields are extended in the air around the spire and only a tiny portion inside the wire material. Thus, in this case it is sufficient to consider only that portion of the fields which are outside the wire material. The air is a very sparse media, and for this reason, the electromagnetic parameters are almost equal to those of the vacuum. So, an approximation which is reasonable and will be consistently made in this work, is to consider the air as having the same properties as the free space ($\varepsilon_{air} \approx \varepsilon_o$ and $\mu_{air} \approx \mu_o$). Even if the fields inside the wire were somehow important, the material properties which shall be considered are constant numbers, unless the frequency is too high or the material too special.

2.4.2-Electromagnetic potentials and gauge

All electromagnetic phenomena must be described by the dynamics of the electric and magnetic fields, which are given as the solutions of the set of Maxwell

equations when supplemented by appropriate constitutive relations. Nevertheless it is frequently useful to define auxiliary functions, usually referred as electromagnetic potentials, in order to turn the calculations manageable. Several problems are easier to solve by obtaining these potentials first and then by calculating the fields from them.

In order to define those potentials, first consider the null divergence of the magnetic field as presented in the set of the Maxwell equations above. Since the divergent of a curl is always equal to zero, we can always write the magnetic field as the curl of another vector field. This other field is usually denoted by $\vec{A}$ and is called the vector potential:

$$\vec{B} = \vec{\nabla} x \vec{A} \tag{5}$$

With this definition, the magnetic field still possesses no divergence in complete accordance with the Maxwell equations set. By plugging this result (Equation 5) into Faraday's law we have:

$$\vec{\nabla} x \vec{E} = -\frac{\partial}{\partial t}\left(\vec{\nabla} x \vec{A}\right) \quad \Rightarrow \quad \vec{\nabla} x \left(\vec{E} + \frac{\partial \vec{A}}{\partial t} \right) = 0$$

The term in parenthesis in the last Equation has a vanishing curl. That means it can be written as the gradient of a scalar function. Thus, we may define a scalar potential V as that function which satisfies the following differential equation:

$$\vec{E} = -\vec{\nabla} V - \frac{\partial \vec{A}}{\partial t} \tag{6}$$

It is possible to obtain an alternative set of equations relating the potentials instead of the fields, as functions of the sources. If that is achieved, one can first obtain the potentials and then retrieve the fields from Equations 5 and 6. In order to do that, Equation 6 is joined with Gauss's law and the following result is obtained:

$$\begin{aligned} \vec{\nabla}.\left(-\vec{\nabla} V - \frac{\partial \vec{A}}{\partial t} \right) &= \frac{\rho}{\varepsilon_o} \\ \Rightarrow \quad \nabla^2 V + \frac{\partial}{\partial t}\left(\vec{\nabla}.\vec{A}\right) &= -\frac{\rho}{\varepsilon_o} \end{aligned} \tag{7}$$

Also, by putting Equations 5 and 6 into Ampère-Maxwell law yields:

$$\begin{aligned} \vec{\nabla} x \left(\vec{\nabla} x \vec{A}\right) &= \mu_o \vec{J} + \frac{1}{c^2}\left[-\frac{\partial}{\partial t}\vec{\nabla} V - \frac{\partial^2 \vec{A}}{\partial^2 t} \right] \\ \Rightarrow \quad \left(\nabla^2 \vec{A} - \mu_o \varepsilon_o \frac{\partial^2 \vec{A}}{\partial t^2} \right) - \vec{\nabla}\left(\vec{\nabla}.\vec{A} + \mu_o \varepsilon_o \frac{\partial V}{\partial t} \right) &= -\mu_o \vec{J} \end{aligned} \tag{8}$$

Equations 7 and 8 express the electromagnetic potentials in terms of the sources. They contain all the information present in the set of Maxwell equations.

Nevertheless, there is still some arbitrariness in the definitions of the potentials making the choice of the functions $\vec{A}$ and V not unique. The lasting freedom which is still present can be removed by noting that we can add to the vector potential the gradient of any scalar function, provided that we subtract the time rate of change of that scalar function in the scalar potential. Then by defining an arbitrary scalar function α, another set of potentials $\vec{A}'$ and V' may be used:

$$\vec{A}' = \vec{A} + \vec{\nabla}\alpha \quad ; \quad V' = V - \frac{\partial \alpha}{\partial t}$$

The change from $\vec{A}$ and V to $\vec{A}'$ and V' is called a gauge transformation. The electromagnetic fields are invariant under this operation. That is, it is possible to show that $\vec{A}'$ and V' provide the same electric and magnetic fields which would be obtained with the original potentials. Since the electromagnetic fields are the only physically meaningful entities, a gauge transformation can be always used without any physical consequence. Once we have this identity: $\vec{\nabla}.\vec{A}' = \vec{\nabla}.\vec{A} + \nabla^2\alpha$, a gauge transformation can be exploited in order to choose the value of the divergence of the vector potential. A common choice for the transformation, commonly known as Coulomb gauge, is to make the divergent of the vector potential to vanish. However the appropriate choice in some circumstances is:

$$\vec{\nabla}.\vec{A} = -\mu_o \varepsilon_o \frac{\partial V}{\partial t} \tag{9}$$

Equation 9 is known as Lorentz gauge and will be the appropriate choice here, being used throughout this work. By plugging Equation 9 into Equations 7 and 8, a considerable simplification is possible and these Equations can be rewritten as:

$$\nabla^2 V - \frac{1}{c^2}\frac{\partial^2 V}{\partial t^2} = -\frac{\rho}{\varepsilon_o} \tag{10}$$

$$\nabla^2 \vec{A} - \frac{1}{c^2}\frac{\partial^2 \vec{A}}{\partial t^2} = -\mu_o \vec{J} \tag{11}$$

The Lorentz gauge is frequently utilized for simplifying Equations 7 and 8 into Equations 10 and 11, which makes the potentials to be treated in the same footing. This symmetry is particularly useful in dealing with relativistic problems.

We then have arrived at two wave equations for the electromagnetic potentials with charges and current distributions acting as sources. At principle, once these initial distributions are known, it is possible so find the potentials through Equations 10 and 11 and then to find the electromagnetic fields from Equations 5 and 6. Unless the distribution of sources is too simple, the general problem of solving Equations 10 and 11 is not easy. General considerations about the method for obtaining the solution of these wave equations are presented on the next subsection.

2.4.3-Time dependent problems and the retarded potentials

The wave equations we intend to solve, accordingly to Equations 10 and 11, present the following structure:

$$\nabla^2\psi(\vec{r},t)-\frac{1}{c^2}\frac{\partial^2\psi(\vec{r},t)}{\partial t^2}=-4\pi f(\vec{r},t) \tag{12}$$

In Equation 12, the term $f(\vec{r},t)$ represents a known source distribution. In order to solve Equation 12 we remove the explicit time dependence by introducing the following Fourier integral representations:

$$\psi(\vec{r},t)=\frac{1}{2\pi}\int_{-\infty}^{\infty}\psi(\vec{r},\omega)e^{-i\omega t}d\omega$$

$$f(\vec{r},t)=\frac{1}{2\pi}\int_{-\infty}^{\infty}f(\vec{r},\omega)e^{-i\omega t}d\omega$$

The inverse transformations are then:

$$\psi(\vec{r},\omega)=\int_{-\infty}^{\infty}\psi(\vec{r},t)e^{i\omega t}dt$$

$$f(\vec{r},\omega)=\int_{-\infty}^{\infty}f(\vec{r},t)e^{i\omega t}dt$$

With these definitions, the Fourier transform $\psi(\vec{r},\omega)$ must satisfy the inhomogeneous Helmholtz wave equation:

$$(\nabla^2+k^2)\psi(\vec{r},\omega)=-4\pi f(\vec{r},\omega) \tag{13}$$

In Equation 13, the wake number k has the following definition: $k=\omega/c$.

Equation 13 is a linear partial differential equation known as *inhomogeneous Helmholtz wave equation*. It can be solved by considering only localized sources first,

and then by using the principle of superposition to write the solution to the general problem as a combination these localized solutions. Consider then the Helmholtz equation for a source localized at the point $\vec{r}\,'$:

$$(\nabla^2 + k^2)G(\vec{r},\vec{r}\,') = -4\pi\delta(\vec{r}-\vec{r}\,') \tag{14}$$

If boundary surfaces are absent, the function $G(\vec{r},\vec{r}\,')$, commonly known as Green's function, can depend only on the difference $\vec{R} = \vec{r} - \vec{r}\,'$. Besides, the point source introduced on Equation 14 demands it must be spherically symmetrical, making it depend only on the distance between the field point and the source point R. This permits further simplifications in the Laplacian operator, and Equation 14 is then rewritten as:

$$\frac{1}{R}\frac{d^2}{dR^2}(RG) + k^2 G = -4\pi\delta\left(\vec{R}\right) \tag{15}$$

Except at the source points themselves ($R = 0$), the Green function must satisfy the following differential equation:

$$\frac{d^2}{dR^2}(RG) + k^2(RG) = 0$$

Its solution being:

$$G(R) = \frac{Ae^{ikR} + Be^{-ikR}}{R} \tag{16}$$

For the region $\vec{R} \to 0$ the delta function on Equation 15 cannot be discarded. However, for this region ($kR << 1$), the second term is negligible in comparison with the first, making the solution easy if the following identity is noted:

$$\nabla^2\left(\frac{1}{|\vec{r}-\vec{r}\,'|}\right) = -4\pi\delta(\vec{r}-\vec{r}\,')$$

Thus the appropriate Green function must be bounded in the region $\vec{R} \to 0$ to

$$\lim_{R\to 0} G(R) = \frac{1}{R}$$

Thus, we conclude that Equation 16 is the solution of Equation 15 provided that $A + B = 1$. We then rewrite Equation 16 for a matter of convenience as:

$$G(R) = AG^{+}(R) + BG^{-}(R) \quad \Rightarrow \quad G^{\pm}(R) = \frac{e^{\pm ikR}}{R} \tag{17}$$

The appropriate values for the constants A and B will depend on the boundary restrictions relative to the time parameter. For a source that is turned on at some time

t=0 it seems intuitive that the G^+ function will be the appropriate choice for the problem because it represents outward propagating waves. Although that choice is convenient, it is not unique. The G^- function may turn the most convenient choice by specifying suitable wave amplitudes at certain boundary times. These different time behaviors can be further investigated by constructing the corresponding time dependent Green functions that must satisfy:

$$\left(\nabla^2 - \frac{1}{c^2}\frac{\partial^2}{\partial t^2}\right) G^{\pm}(\vec{r},t,\vec{r}',t') = -4\pi\delta(\vec{r}-\vec{r}')\delta(t-t')$$

By using the Fourier transformations as defined at the beginning of this subsection, we conclude that the source term is rewritten as $-4\pi\delta(\vec{r}-\vec{r}')e^{i\omega t'}$. Thus the time dependent Green functions are simply given as $G^{\pm}(R)e^{i\omega t'}$. In order to make the time dependence explicit, the Fourier transformations are used again and we obtain the following time dependent Green functions:

$$G^{\pm}(\vec{r},t,\vec{r}',t') = \frac{1}{2\pi}\int_{-\infty}^{\infty} \frac{e^{\pm ikR}}{R} e^{i\omega(t'-t)} d\omega$$

After integrating the last equation, the Green function is explicitly given as:

$$G^{\pm}(\vec{r},t,\vec{r}',t') = \frac{\delta\left(t' - \left[t \mp \frac{|\vec{r}-\vec{r}'|}{c}\right]\right)}{|\vec{r}-\vec{r}'|} \tag{18}$$

The Green function G^+ is called the *retarded Green function.* That is because the argument of the delta function ensures that an effect observed at a position $\vec{r}$ and time t is caused by the action of a source at a distance R away, at an anterior time $t' = t - R/c$ also known as retarded time. In a similar manner, the function G^- is called the *advanced Green function*. This time dependence reflects the fact that the electromagnetic waves can only propagate with a finite speed given by $c = 1/\sqrt{\mu_o \varepsilon_o}$ at the free space.

We had shown the solution of Equation 14, which is essentially a particular case of Equation 13 for localized sources. By superimposing these solutions we may actually represent the case of a distributed source and, with this, a particular solution of Equation 13 is written as:

$$\psi^{\pm}(\vec{r},t) = \iint G^{\pm}(\vec{r},t,\vec{r}',t') f(\vec{r}',t') d^3r' dt'$$

The general solution of Equation 13 was not specified yet because we still need to add the general solution of the associated homogeneous wave equation. In order to do that, it is necessary to specify the physical problem by choosing between the retarded or advanced Green function.

Then we consider first the problem of a wave $\psi_{\text{hom}}(\vec{r},t)$ that satisfies the homogeneous wave equation and is assumed to always have existed ($t \to -\infty$). Also there is a source that is quiescent until the time $t'=0$ when it is turned on, and for this reason, generates waves of its own. The complete solution for this case is written as:

$$\psi(\vec{r},t) = \psi_{\text{hom}}(\vec{r},t) + \iint G^{+}(\vec{r},t,\vec{r}',t') f(\vec{r}',t') d^3r' dt' \tag{19}$$

In this case, the presence of the Green function G^{+} guarantees that no contribution can come from the integral before the source is turned on.

The other situation is to consider that at remotely later times ($t \to +\infty$) a wave $\psi_{\text{hom}}(\vec{r},t)$ is specified as the solution to the homogeneous wave equation. Also, the source had always been functioning when it is turned off at $t'=0$. Then the complete solution for this case is given as:

$$\psi(\vec{r},t) = \psi_{\text{hom}}(\vec{r},t) + \iint G^{-}(\vec{r},t,\vec{r}',t') f(\vec{r}',t') d^3r' dt' \tag{20}$$

In this second case, the function G^{-} guarantees that no signal can arise from the source after it shuts off.

The most common case is that described by Equation 19. The physical situation represented with this is the case of a source which is quiescent being turned on at some specific time. As this is the case we shall study in this work, we focus our attention to this particular representation. By inserting explicitly the retarded Green function on Equation 19, we are left with the following expression for the solution of this problem:

$$\psi(\vec{r},t) = \psi_{\text{hom}}(\vec{r},t) + \int \frac{\left[f(\vec{r}',t') \right]_{ret}}{|\vec{r}-\vec{r}'|} d^3r' \tag{21}$$

In Equation 21 the brackets $\left[\ \right]_{ret}$ means that the time t' must be evaluated at a retarded time, that is, $t' = t - |\vec{r}-\vec{r}'|/c$.

Now we may return to Equations 10 and 11 which were the motivation for this subsection. By recurring to the result expressed on Equation 21, we know how to write the solutions of Equations 10 and 11 by simple comparison. These are given below:

$$V(\vec{r},t) = V_{\text{hom}}(\vec{r},t) + \frac{1}{4\pi\varepsilon_o}\int \frac{\left[\rho(\vec{r}',t')\right]_{ret}}{|\vec{r}-\vec{r}'|} d^3r' \tag{22}$$

$$\vec{A}(\vec{r},t) = \vec{A}_{\text{hom}}(\vec{r},t) + \frac{\mu_o}{4\pi}\int \frac{\left[\vec{J}(\vec{r}',t')\right]_{ret}}{|\vec{r}-\vec{r}'|} d^3r' \tag{23}$$

Equations 22 and 23 express the scalar and the vector potential which can be obtained once a particular initial distribution of charges (ρ) and also of currents ($\vec{J}$) are specified everywhere in the space, in a retarded time. The solution to the homogeneous wave equation ($V_{\text{hom}}(\vec{r},t)$ and $\vec{A}_{\text{hom}}(\vec{r},t)$) also needs to be specified.

Once the initial distribution of charges and currents is known, it is possible to calculate the potentials through the use of Equations 10 and 11. Nevertheless, it may be easier to specify those sources at a retarded time to obtain the potentials from Equations 22 and 23 instead. The fields can then be retrieved through Equations 5 and 6.

2.5-Some fundamental electromagnetic effects and their impedances

In this section we present the derivation of some fundamental electromagnetic effects and their resulting impedances. The starting point is the set of Maxwell equations and the definition of electromagnetic potentials as they represent useful tools. The effects which shall be derived are nowadays largely applied in the fabrication of a countless amount of devices which are present in our everyday lives and constitute a basis for modern electronics. The impedance of the basic circuit elements of electronics will be presented. Electromagnetic phenomena are seminal to a wide class of materials and geometries and are of immensurable relevance in the field of physics and engineering.

Much of the design and analysis of devices are performed by use of lumped-circuit elements modeling. In this case, the components used to describe real devices present characteristic impedances and interact with each other through the use of negligible impedance paths which couple them electromagnetically. Several passive devices can be satisfactorily represented in a broad frequency range by a specific idealized lumped circuit element or by a proper combination of a few of them. Some idealized circuit elements are of widespread in basic electronics; they are called the resistor, the inductor and the capacitor (R/L/C).

The linking between two components in an electrical circuit is most often assumed to possess negligible impedance. This however may not be strictly true, especially if the lengths of these connections are large. However, for the majority of cases a large linking can also be modeled by a proper combination of those three classical elements. For other cases another approach might be necessary, as for example by considering distributed impedances rather than localized ones, as in the case of transmission lines.

Another approximation frequently made in order to calculate impedances is to consider that the size of an element is negligible in comparison with the wavelength of the electromagnetic field. If that is reasonable, then the fields can be regarded as *quasistatic.* This means that, although time varying, the fields have a spatial distribution which is essentially the same as if they were static. If the element is rather large, the lumped circuit modeling can still be satisfactory but, the distribution of fields inside the element must be taken into account in a more rigorous way.

2.5.1-The resistance

Before the seminal work of George Ohm, Henry Cavendish performed by the year of 1781, several experiments with Leyden jars and glass tubes filled with saline solutions. He studied the propagation of electricity through those systems by varying the geometry (lengths and diameters). At his time he did not have tools to quantify electrical quantities except his own body sensations. This way, he measured the intensity of flow of electricity by observing how strong a shock he felt when closing the circuit with his own body. These results were only known after their through study and publication by Maxwell in the year of 1879. In the years of 1825 and 1826 George Ohm conducted a series of experiments using Voltaic Piles, and later using thermocouples in order to generate more stable voltage sources. He used Galvanometers to measure electric current and closed his circuits with different material, lengths and diameter wires. In order to provide a theoretical explanation to his work Ohm inspired himself on Fourier's works on the conduction of heat. In 1827 Ohm published his work establishing the proportionality between voltage and current, but he suffered hostility from the critics. By the decade of 1850's Ohm's law was considered widely proved and useful to applications such as telegraph system design as stated by Samuel Morse in

1855. A brief review on the history of Ohm's law can be found on the work of Shedd [44].

In order to present the effect studied by Ohm, we consider a short piece of conducting material for which a potential difference is applied between its extremities as illustrated by Figure 4:

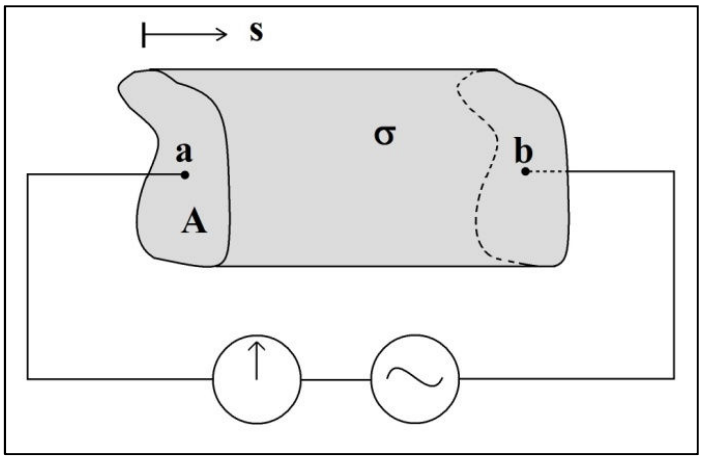

Figure 4: Piece of conducting media submitted to an applied potential difference.

Conductors are usually defined as those materials satisfying a constitutive relation, which is frequently referred as Ohm's law. This relation states that, as consequence of the applied potential difference, a current density is established and is proportional to the resulting electric field. The constant of proportionality (σ) is called the conductivity:

$$\vec{J} = \sigma \vec{E} \tag{24}$$

Consider first that the applied potential difference is constant in time, in a way that the potentials and, as consequence, the fields are also static. Then, by making the time rate of change of the vector potential null in Equation 6, we can perceive that the electric field can be obtained simply from the gradient of the applied signal ($\vec{E} = -\vec{\nabla} V$). In an equivalent manner, we can argue that the electrical potential difference can then be written as a path integral of the electric field along the material length:

$$V(b) - V(a) = -\int_a^b \vec{E}.d\vec{s} \tag{25}$$

By joining Equations 24 and 25 we can rewrite this potential difference as

$$V_R \equiv V(a) - V(b) = \int_a^b \frac{\vec{J}.d\vec{s}}{\sigma} = I \int_a^b \frac{ds}{\sigma A} \equiv IR \tag{26}$$

On the last step of Equation 26 the current density was assumed to be homogeneous, that is, it cannot change from one point inside the material to another. This is the only way of conserving the electrical charge inside the sample, at least in this electrostatic approximation.

Although Equation 26 was derived by assuming an electrostatic situation, it may be valid even for the case of time varying fields. This is true if the time rate of change of the fields is not so large, that is, if the applied frequency is well below the plasma frequency of the conducting material. In this case we have assumed that the length of the device is much smaller than the wavelength of the fields, characterizing the *quasistatic* approximation. This means that the fields instantaneously have the spatial distribution as they would have in the static case, and the time dependence is included by simply multiply the static fields by the harmonic factor $e^{i\omega t}$. This motivates us to define, in a more general way, the resistor as that circuit element for which the potential difference is instantaneously proportional to the electrical current inside it. The constant of proportionality (R), which was defined on Equation 26, is called the resistance and depends upon the conductivity as well as the geometry of the material. This relation is written down below:

$$V_R(\omega,t) = RI_R(\omega,t) \tag{27}$$

Equation 27 tells us that the time dependence of the current will be just the same of the applied potential difference. From this, we can readily see that the impedance of a resistor is independent of the applied frequency and is simply given by the constant resistance value:

$$Z_R \equiv \frac{V_R(\omega,t)}{I_R(\omega,t)} = R \tag{28}$$

Notice that the impedance of a resistor is a real number, that is, its phase angle is null. This means, from the definition of Equation 4, that the applied voltage and resulting current are in phase with each other.

A more precise justification for this *quasistatic* approximation inside good conductors can be obtained by considering the Drude model for the conductivity [45]. By the year of 1900, Drude presented a model for the electronic conductivity of a material. His work attained great success in explaining the conductivity of metals in a relative broad frequency range. He applied the kinetic theory to the electrons in the material, which he assumed to be detached from the atoms and behave similarly to a gas

around positively and immobile positive ions. It turns out that in practice, this free electron model is good enough for the vast majority of metals and for the frequency range of interest in this work (MHz). Thus, for the cases which we shall treat here, the conductivity will always be considered to a real, frequency independent and positive number.

2.5.2-The inductance

Inductance is the ability of a conductor which is carrying a time changing current, to induce voltages inside itself (self-inductance) and on nearby conductors (mutual-inductance). This property can be deduced from a few fundamental observations. The first connection between magnetism and electricity was discovered by Oersted in 1820. He observed that a steady electrical current generates a magnetic field around it. He noticed that by observing the needle of a compass to place itself perpendicularly to a nearby current carrying wire. Electromagnetic induction was discovered independently by Michael Faraday in 1831 and Joseph Henry in 1832. Faraday provided demonstrations of electromagnetic induction by wrapping two wires on opposite sides of an iron made torus. Then he connected one of the wire wrappings to a galvanometer, and the other to a battery. He was able to measure current transients as he connected and disconnected the battery to the system. Faraday explained electromagnetic induction by introducing the concept of lines of force, but his ideas were rejected mostly because they were not mathematically formulated. Those ideas of lines of force were used later by James Clerk Maxwell in order to formulate a mechanical model of electromagnetism. A critical examination of the electromagnetic induction history can be found at the reference [46].

In order to apply the potential difference across two points of a piece of material as discussed on the last subsection, it is necessary to link the material to a battery or a generator. The usual way to do that is through the use of a loop of good conducting wire. By good conducting we mean a material with an infinite conductivity, in such a way that the resistance of the wire is essentially zero. The concern however, is the possibility of introducing extra impedances, other than wire resistance. This is because the Ampère-Maxwell's law states that a magnetic field which surrounds the wire will be produced. In turn, Faraday's law states that the time rate of change of the flux of that

magnetic field will induce additional electric fields inside the wire, changing the current and then the impedance of the loop.

This way, we now take a look at a closed path of conducting wire alone, and see what impedances it can produce. Consider that a single spire (closed loop of wire) is carrying an alternate current. For the sake of simplicity this loop is assumed, without loss of generality, to lie in a plane as illustrated on Figure 5 below:

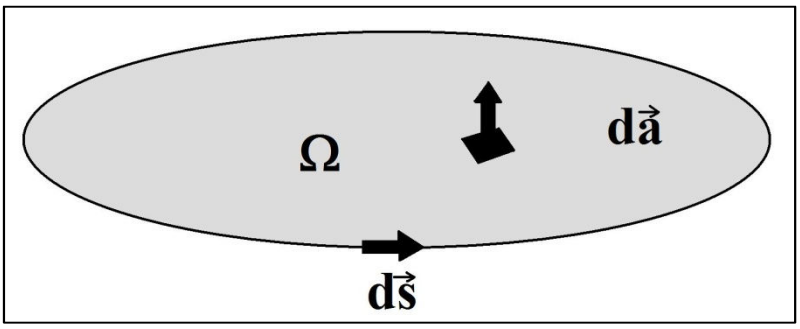

Figure 5: Single wire loop.

Then define the simplest surface Ω which lies in the loop plane and is bounded by the contour of the loop. By use of Faraday's law it is possible to calculate the time rate of change of the magnetic flux inside this surface:

$$\int_{\Omega}\left(\vec{\nabla}x\vec{E}\right).d\vec{a} = -\frac{\partial}{\partial t}\int_{\Omega}\vec{B}.d\vec{a} \tag{29}$$

The symbol $d\vec{a}$ on Equation 29 represents an element of area inside the surface Ω as depicted on Figure 5. By use of Stokes's theorem we can change the flux of the curl of the electric field by the integral path of that field along the loop path. Also, the Ampère-Maxwell law can be used to calculate the magnetic field and thus its flux on the surface Ω. The term proportional to the time rate of change of the electric field in Ampère's law is divided by the square of the speed of light, being negligible if compared to the time rate of change of magnetic field of Faraday's law. This way we may assume that the magnetic field and so, its flux, is proportional to the current inside the wire. Then Equation 29 is rewritten as:

$$V_L \equiv \oint \vec{E}.d\vec{s} = -\frac{\partial}{\partial t}\int_{\Omega}\vec{B}.d\vec{a} \equiv -\frac{\partial}{\partial t}\left(LI\right) \tag{30}$$

This motivates the definition of another circuit element called the inductor. For this element, the potential difference between its terminals is proportional to minus the time rate of change of the current. The constant of proportionality which was defined in

Equation 30 depends upon the detailed geometry of the loop and is called the inductance (L). We may then define an inductor as that circuit element which obeys the following relation:

$$V_L(\omega,t) = -L\frac{dI_L(\omega,t)}{dt} \quad \Rightarrow \quad I_L(\omega,t) = -\frac{V_o}{i\omega L}e^{i\omega t} \tag{31}$$

In Equation 31 the harmonic time dependence which was introduced by Equation 2 was assumed. This way, the impedance of an inductor can be readily written as

$$Z_L(\omega) = i\omega L \tag{32}$$

A current carrying loop of wire can then be modeled by using an inductor element. It is clear from Equation 32 that the impedance of this system increases with the applied frequency and also possesses a phase angle equal to $\pi/2$. On the above analysis we have considered the case of a thin wire, that is, we have only considered the fields outside the wire. The resulting inductance from this calculation is commonly denominated as external inductance. It may be necessary, for some cases, to consider the fields inside a non-zero thickness wire. The inductance resulting from that calculation is denominated the internal inductance.

A device that is of common usage in electronics is the coil. A coil is constructed by wrapping a wire around some support in order to produce several current loops instead of the single loop as discussed above. The aim of having more than one current loop is to exacerbate the effect produced by Faraday's law, since the flux of the magnetic field is now roughly multiplied by the number of turns, and so is the induced potential difference.

2.5.3-The capacitance

Until now we have not explored a very useful property that can be easily observed at several configurations; the capacitance. This property describes the ability of a body to accumulate electrical charge. In addition to support electrical currents, a material may store electrical charge when submitted to a certain electric potential. A device which is build with this purpose is called a capacitor. The invention of the capacitor is attributed to a German scientist named Ewald Georg von Kleist who worked in end of the year 1745, and observed that charge could be accumulated by connecting an electrostatic generator to a volume of water in a hand held glass jar. In this case the water volume and the hand acted as conductors and the glass in between

was the dielectric. Several months later, Pieter van Musschenbroek, a Dutch professor at the University of Leyden independently made up a similar device named Leyden Jar which is sometimes credit as the first capacitor [47].

In practice the term capacitance is often used to refer to the mutual capacitance between two conductors, but a self-capacitance may also be defined as the amount of charge that is added to a conductor in order to elevate its electrical potential by one unit. The mutual capacitance or, in short, the capacitance of a pair or conductors is defined to be the ratio between the charge accumulated on the conductors and the potential difference raised in order to build that separation of charges. By taking the time derivative of this relation, we can write the following differential equation which relates the time rate of change of the potential difference and the current in the system:

$$C \equiv \frac{Q}{V_C} \quad \Rightarrow \quad \frac{dV_C(t,\omega)}{dt} = \frac{1}{C} I_C(t,\omega) \quad \Rightarrow \quad I_C(t,\omega) = i\omega C V_o e^{i\omega t} \tag{33}$$

The harmonic time dependence was assumed just as we have made on the resistance and the inductance cases. A capacitor is then defined as that circuit element for which the current is proportional to the time rate of change of the potential difference across its terminals. The constant of proportionality is the reciprocal of the capacitance (C). This number is also a geometrical property since it also depends on the exact spatial configuration of the conductors. The concept of capacitance may be also attributed not as a simple result of some particular geometrical distribution of charges, but in a more involved way. That is the case of quantum capacitance [48], which arises from systems possessing a low density of states such as a two-dimensional electronic system as a semiconductor surface or graphene [49]. We only consider in this development the geometrical capacitance arising from a charge distribution. By using the capacitance definition provided on Equation 33, the impedance of a capacitor can be written as

$$Z_C(\omega) = \frac{1}{i\omega C} \tag{34}$$

Note that the impedance of a capacitor decreases with the applied frequency and possess a phase angle equal to $-\pi/2$. The most common device that explores this property is the parallel plate capacitor. This device is built by using two plane and parallel conductors for which the potential difference is applied. These conductors are usually separated by a slab of dielectric material.

2.5.4-Lumped circuit elements modeling

A great sort of linear passive devices can be modeled by using one of the circuit elements described above. However, in some cases it is necessary to use a proper combination of a few basic circuit elements in order to represent a real device. Take a piece of conducting material as discussed on subsection 2.5.1 for example. Even in that situation, a changing magnetic field will surround the material and, as consequence, induce potential differences along its axis. For this reason, an inductive character is also expected. The point however, is that for a short piece of material, this effect will be small when compared to the resistance effect. On the other hand, if the frequency is so high that the time rate of change of the magnetic field is large enough, considerable potential differences would be induced in the material and the inductive character would certainly be observed, even for a short length material. The same applies to the loop current discussed on subsection 2.5.2. For this configuration it is possible to apply a signal of such a small frequency, that the inductive character would be small in comparison with the resistance effect.

It is of common usage to construct a model consisted of an electrical circuit comprising several basic circuit elements linked to each other in order to represent real devices. Such a model is frequently referred as the lumped circuit model or the equivalent circuit. It is possible to associate these basic circuit elements by linking them in a way to apply the same potential difference to the components of the set (parallel association) or in a way to drive the same current to these components (series association). The elements are assumed to be connected by paths of negligible impedance. In order to perform the analysis of a circuit association of elements, there are basic circuit rules which provide equations relating potential differences and currents within it. These rules were introduced by Kirchhoff in 1845 [50]. Widely used on Electrical Engineering, they are frequently called Kirchhoff's circuit laws. One of the Kirchhoff laws is based on the principle of the conservation of the electrical charge. It states that the algebraic sum of the currents in a node of the circuit is equal to zero. The other Kirchhoff law states that the electrical potential drops inside each element, plus eventual raises in it which are caused by the presence of sources, is also equal to zero, for a closed circuit path. By combining these two rules it is an easy matter to check that the impedance of a series association is given by the sum of the individual impedances

of the elements ($Z_s = Z_1 + Z_2$) and that the impedance of a parallel association is given by the inverse of the sum of reciprocals of individual impedances ($Z_p^{-1} = Z_1^{-1} + Z_2^{-1}$).

These circuit laws must be used with great care in a practical circuit, because it is easy to find situations for which they are violated. The reason for that is that these rules assume that the linking between the circuit elements possess negligible impedance, and that may be unrealistic. For example, the sum of voltages in a closed circuit path is not equal to zero in the case of alternating currents. That is because the changing magnetic field produced by the devices, and also by the connecting wires themselves, will induce potential differences on these linking wires. Thus, for this kind of circuit, the cabling impedance cannot be ignored. However, the impedance of the cables can be frequently also modeled by some proper combination of circuit elements which are added into the modeling circuit. Then a proper model will generally comprise circuit elements designed to describe the devices and some other elements intended to describe the cabling connections. This way, the Kirchhoff circuit laws are then applicable to the correct modeling circuit.

2.5.6-Skin effect

An interesting effect happens when measuring the electrical resistance of a conductor with an alternating signal. The result actually depends on the chosen frequency, being larger for higher frequency values. This phenomenon is present even in the *quasistatic* approximation, as discussed on subsection 2.5.1. That is, even for frequencies which are not so high as to change the conductivity of the material we can observe a frequency dependent resistance. What happens in this case is that the electric field distributes itself into smaller portions of the conductor as the frequency augments. We know from Ohm's law that the current density is proportional to the electric field. Thus, the current density will also distribute itself into smaller regions turning the area available to transport smaller, and the resistance larger. This is called the skin effect.

The charge density inside the volume of a perfect conductor, in an electrostatic situation is null. That is because if a charge is placed inside it, the electric field generated by it will act on the free electrical charges (electrons in a metal) which are inside the conductor by definition. This will establish a current density which will redistribute the charge until it completely vanishes. As a consequence, the electric field

itself also vanishes inside the volume of this conductor. The electron mobility inside a typical conductor is so high that this process generally occurs much faster than the reciprocals of the frequencies of the exciting signals. All interesting phenomena will lie on the conductor surface were the excess of charge (if there is one) is placed. This analysis is also valid in the *quasistatic* approximation, being also true for low frequency harmonic signals, as discussed in the subsection 2.5.1.

In order to investigate this phenomenon in a more precise way, consider a linear and isotropic conducting material for which an alternating signal is applied. The electric field inside it can be written as:

$$\vec{E}(\vec{r},\omega,t) = \vec{E}_o(\vec{r},\omega)e^{i\omega t} \tag{35}$$

In order to evaluate the distribution of this electric field inside the media, we invoke the Faraday's law of induction and apply the curl operator at both sides of it:

$$\vec{\nabla}x(\vec{\nabla}x\vec{E}) = \vec{\nabla}(\vec{\nabla}.\vec{E}) - \nabla^2\vec{E} = -\frac{\partial}{\partial t}(\vec{\nabla}x\vec{B})$$

There may have no charges inside a good conductor, and by use of Gauss's law we see that the electric field must possess no divergence. By adding that fact and also by including the information on Ampère-Maxwell law, we have:

$$\nabla^2\vec{E} = \frac{\partial}{\partial t}\left(\mu\vec{J} + \frac{1}{c^2}\frac{\partial\vec{E}}{\partial t}\right)$$

In order to further simplify the result given above, note that Equation 24 is frequently used to define a conductor. In other words, in a conductor, the current density is linearly proportional to the electric field (Ohm's law). Also note that for the simple time dependence assumed on Equation 35, the derivative operation is performed by simply multiplying the fields by $i\omega$. This results in:

$$\nabla^2\vec{E} = \left(i\omega\mu\sigma - \frac{\omega^2}{c^2}\right)\vec{E}$$

For the frequency range of interest (maximum of dozens of MHz), and for the vast majority of conductors such as copper at room temperature ($\sigma = 5.96x10^7\,\Omega^{-1}m^{-1}$ and $\mu \approx \mu_o$), the following relation is valid: $\omega\mu\sigma \gg \omega^2/c^2$. This enables us to neglect the second term in the parenthesis of the equation above. In the case of copper, the second term is as smaller as billionths of the first, even at frequencies in the range of GHz. This simplification results in:

$$\nabla^2 \vec{E} = i\omega\mu\sigma\vec{E} \tag{36}$$

Consider the differential Equation 36 for the case of a plane conductor extending itself to the infinity as well as having an infinite thickness. That is, consider that in a Cartesian system of coordinates, the conductor extends itself along the half-space (x>0) region. If the electric field points in the z direction and we assume no variations in the y and z directions, then we have

$$\frac{d^2\vec{E}_o}{dx^2} = i\omega\mu\sigma\vec{E}_o \quad \Rightarrow \quad \vec{E}_o = \vec{E}_{oz}e^{-\sqrt{i}\frac{x}{\delta}} \tag{37}$$

$$\delta = \frac{1}{\sqrt{\omega\mu\sigma}} \tag{38}$$

The parameter δ is called the skin dept of the radiation. It measures how deep an electromagnetic field can penetrate inside a conductor. The used geometry of a plane conductor is useful for treating the case of the incidence of electromagnetic radiation on a metallic surface, for example.

In spite of the fact that Equations 37 and 38 are only exact for a "semi-infinite" plane conductor, this result may be a good approximation for a great number of cases, including some problems for which the conductor is not plane, as in the case of a wire for example. For high frequency values the skin depth may be much smaller than the diameter and curvature of the wire, in a way that the conductor may be regarded as an infinitely thick plane. The resulting electric field has a vanishingly amplitude as it propagates inside the conductor along a typical distance of a few δ as can be seen from Equation 37. For low frequency values, the skin dept may be so large that the filed may be regarded as homogeneously distributed. As reference values, take for example, copper at the frequency values of 1Hz and 100MHz. Then the skin dept values at those frequencies are approximately: $\delta(1Hz) \simeq 5cm$ and $\delta(100MHz) \simeq 5\mu m$.

Let us return to the experiment of measuring the electrical resistance of a metallic wire. We assume that an alternating current is driven through a round straight wire. Now, the natural choice for the system of coordinates is the cylindrical one. The axis of this conductor, and consequently its current, are chosen to lie on the z axis and no variations with the z or the polar coordinate ϕ are allowed. By symmetry we can argue that no variations with the polar coordinates are expected, but the dependence with the axial coordinate is discarded by assuming that no charges can be build inside a

conductor. Then, we may use Equations 36 and 24 to write down an expression for the current density inside the wire:

$$\nabla^2 \vec{J}_z = i\omega\mu\sigma\vec{J}_z \tag{39}$$

With the choice of cylindrical coordinates and the above specified symmetry considerations, Equation 39 may be rewritten as:

$$\frac{d^2 J_z}{dr^2} + \frac{1}{r}\frac{dJ_z}{dr} = \frac{i}{\delta^2} J_z$$

The solution to the above equation is a combination of the Bessel functions of the first and second type. Since the second type Bessel function has no boundary at the point $r = 0$, it must be excluded from the solution of the problem. Thus we may write the current density inside the wire as:

$$J_z = \alpha J_o\left(\frac{i^{3/2}}{\delta} r\right) \tag{40}$$

Where J_o is the zero order Bessel function of the first kind. The constant α can be found by demanding that the flux of the current density across the wire to be the total electrical current. For a round wire of radius a we then have:

$$I = \int_0^{2\pi}\int_0^{a} \alpha J_o\left(\frac{i^{3/2}}{\delta} r\right) r dr d\phi \quad \Rightarrow \quad \alpha = \frac{I}{2\pi a\delta}\frac{i^{3/2}}{J_1\left(\frac{i^{3/2}}{\delta} a\right)} \tag{41}$$

A plot of the modulus of the current density as function of the wire radius, for certain frequency values, gives us a clue on how the current is distributed along the cross sectional area of the wire. Figure 6 below displays the current density inside a 1mm radius copper wire carrying a harmonic electrical current of amplitude 1A, for several frequency values:

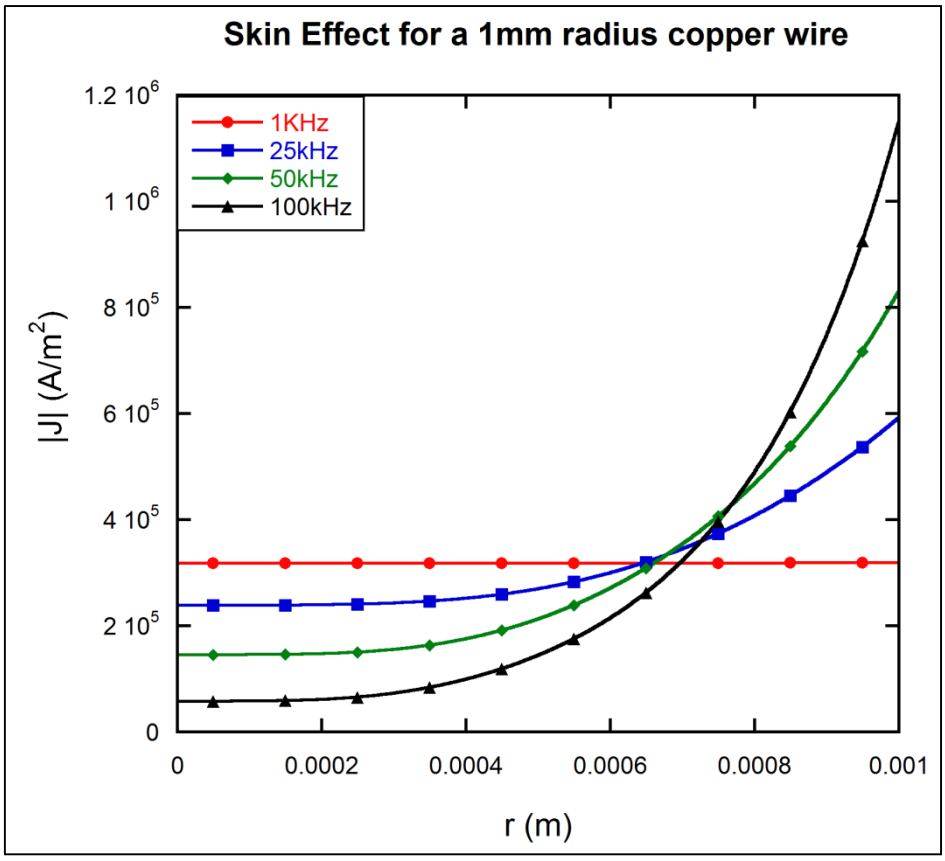

Figure 6: Calculated modulus of current density for a 1mm radius copper wire carrying a harmonic current of amplitude 1A , for the frequencies of 1KHz (●), 25KHz (■), 50KHz (♦) and 100KHz (▲).

From Figure 6 we can see that, as the frequency increases, the current is expelled towards to the wire surface ($r = 1mm$). This results in an increase of impedance since the effective area available to transport gets smaller as the frequency increases.

If the wire impedance is desired, the ratio between voltage and current is needed. Nevertheless, a more general result is the impedance per unit length of wire. This quantity is simply the ratio between the electric field and the current. Even then, it would be necessary to define an r-dependent distributed impedance function and to consider a concentric ring shaped element of area where the current density is a constant, in order to take into account the variation with the coordinate r. In order to avoid that complication we may take a reference point at the border of the wire ($r = a$), were the current tends to be concentrated on. Thus we define the skin impedance as the impedance per unit length of the wire as given by

$$Z_{skin}(\omega) \equiv \frac{E_z(a)}{I} = \frac{i^{3/2}}{2\pi a \delta \sigma} \frac{J_o(i^{3/2} a/\delta)}{J_1(i^{3/2} a/\delta)} \tag{42}$$

Equation 42 expresses an approximation for the impedance of a round wire capable of presenting the skin effect. The measured impedance may be lower than that calculated, once the regions of small r values also contribute to the total current and represent parallel impedances that were neglected. But at least for high frequency values, when the effect is exacerbated and almost all of the current is nearly on the surface of the wire, Equation 42 is a good approximation. Figure 7 below illustrates the skin effect for the case of the 1mm diameter copper wire. There, the real and imaginary parts of the impedance of this wire were calculated using Equation 42 and plotted as function of the applied frequency:

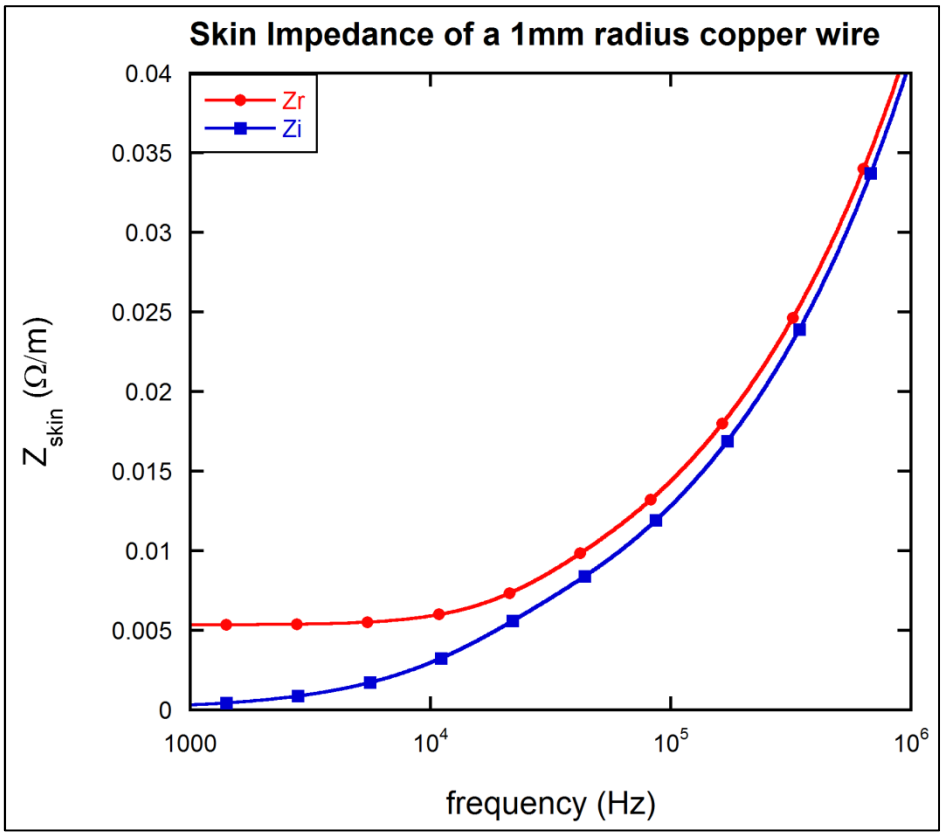

Figure 7: Real (●) and imaginary (■) parts of the Skin Impedance of a 1mm radius copper wire as function of the applied frequency.

By examining Figure 7 we can check that the modulus of the impedance increases with the applied frequency because both the real and imaginary parts are ascending functions. That picture is consistent with the interpretation provided from the analysis of Figure 6, that is, as frequency increases the effective area available to transport becomes smaller and the impedance increases.

2.5.7-Diffusional processes: the Warburg impedance

The electromagnetic effects in a circuit are related to several thermodynamic processes which occur inside it. As a simple example, when conduction takes place, part of the work done on the charges by the electric field is converted into heat by random collisions of these charges in the structure of the material, as pictured by Drude and cited on section 2.5.1. Thus, even in the simple case of a piece of current carrying material it may be insufficient just to solve Maxwell equations in order to explain the whole system dynamics. That is because the temperature changes induced by the energy coming from the electric field may alter material properties and, in turn, change the electric transport characteristics. Nevertheless, for the case of a current carrying wire, the electrical power is sometimes so small that the heat is readily dissipated to the environment and the temperature is approximately constant in time. That is especially true for slow amplitude signals and currents, as in the case of the measuring the impedance.

In some situations however, a particular thermodynamic process may be of great relevance or even be the dominant aspect. That is the case of diffusion in some electrochemical systems. Inside a metal, the charge carriers (electrons) have such a high mobility that the time needed for any excess of charge to redistribute itself on the surface of the conductor is generally too small. This time is frequently much smaller than the reciprocal of the frequencies of the applied signals. On the other hand, electrochemical systems generally present typical charge carriers which have significantly smaller mobility (ions). This way, when applying a potential difference between two points of a salty water volume for example, the response current will be limited by ionic diffusion. Instead of readily responding to the electric field like the electrons in a metal, the ions will suffer from the random thermal collisions with the water molecules. These random collisions will generate a diffusion current density in order to stabilize the concentration gradients generated by the electric field, as stated by Fick's law: $\vec{J}_{diff} = -D\vec{\nabla}C$ [51]. The parameter D is called the diffusion coefficient.

Warburg was the first to extend the concept of impedance to electrochemical systems [12]. He derived the impedance of a system undergoing a diffusional process. By using Fick's law and also the continuity equation: $\vec{\nabla}.\vec{J} + \partial C/\partial t = 0$, it is possible to derive an equation for the space and time dependent concentration field C. The result is

sometimes called the diffusion equation, the heat equation or still the second Fick's law. This result is provided below:

$$\frac{\partial C(x,t)}{\partial t} = D\frac{\partial^2 C(x,t)}{\partial x^2}$$

For a harmonic excitation, it is reasonable to expect also a harmonic time dependent concentration field such as $C = C_o e^{i\omega t}$. Thus, it is possible to solve the diffusion equation by considering the Fourier representation and changing it to the frequency domain as was done with the wave equation, in subsection 2.4.3. The definition of an appropriate Green function, corresponding to an initial localized source would be necessary. The solution to this problem in the frequency domain is presented as follows:

$$C(\omega, x) = C_o \exp\left(-\sqrt{\frac{i\omega}{D}}x\right)$$

From the form of this solution it is possible to note that, for an applied frequency ω, the diffusing particles will undergo a distance of about $\lambda = \sqrt{D/\omega}$ in a characteristic time of about the reciprocal of ω. Thus, by making a simple analogy with Equation 26, we may define a diffusion-generated impedance. We argue that the impedance advent from this diffusion process must have a modulus equal to $|Z_W| = \lambda/\sigma A$. That is, its modulus is that of a resistor having a length of about the typical diffusion length λ.

The conductivity of an electrochemical system is usually written as function of the ionic mobilities, concentrations and electrical charges. Consider then a single ionic species whose electrical charge is given by $q = \upsilon e$, in which υ is the ionic valence and e the fundamental electrical charge. The conductivity is then given by the product of mobility, charge, and ionic concentration: $\sigma = \mu |q| C$. Another useful result is Einstein-Smoluchowski relation [52]. It states that the ratio between mobility and diffusion coefficient is proportional to the ratio of electrical and thermal energies $\left(\mu/D = e/k_B T\right)$. It is also possible to show that this diffusive impedance possesses a constant phase angle equal to $-\pi/4$. By joining all these results, the whole expression for the diffusive impedance is given by

$$Z_W = \frac{W}{\sqrt{i\omega}} \quad ; \quad \mathrm{W} = \frac{k_B T}{|\nu| e^2 CA\sqrt{D}} \tag{43}$$

The impedance of Equation 43 is called the Warburg impedance. It is frequently used in a lumped circuit elements model, combined with other elements such as capacitors and resistors, in order to describe the full electrical behavior of an electrochemical cell [53].

2.5.8-Newmann's formula for the inductance of a spire

A case of great interest is that of a filamentary current. This system may be defined by considering a current carrying material which is much longer than wide or tick, as is frequently the case of a conducting wire. This physical situation is very common and will be of particular interest in this work. For this reason, we present here a usual approach to this calculation due to Newmann. On Chapter 3 we shall consider in detail the impedance of a thin spire which is essentially a conducting wire presenting a filamentary current. There, we derive a more general impedance formula for the impedance of a spire. By introducing the presence of undamped current waves along the length of the spire we generalize Newmann's result, extending the impedance real part values to the negative range.

Consider then two closed loops of filamentary currents, close to each other. From Ampère's law, the magnetic field produced by Loop 1 is proportional to the current I_1 and the magnetic field from Loop 2 is proportional to the current I_2. Then some of the magnetic field lines of Loop 1 pass through the Loop 2 and vice-versa, as illustrated on Figure 8 below:

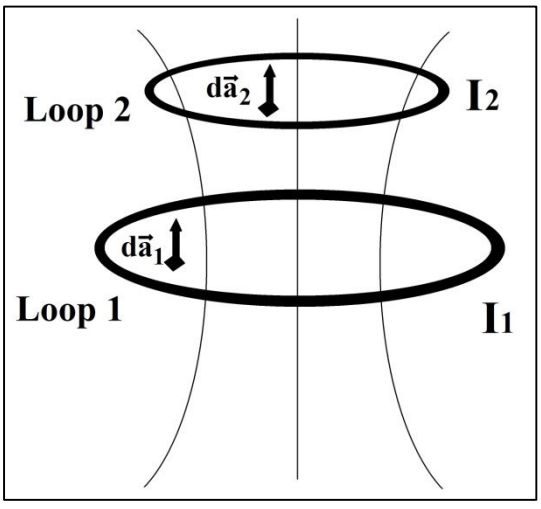

Figure 8: Two current carrying loops of wire. The magnetic field produced from one loop intercepts the other one.

We have already defined the inductance as the proportionality between the magnetic field and current in section 2.5.2 by Equation 30. In that situation the magnetic flux across the loop surface was due to the current loop itself. For this reason, the inductance of that configuration is called the self inductance. A difference scenario is displayed on Figure 8. Consider then the magnetic field $\vec{B}_1$ which is produced by Loop 1. The flux of this field through the surface of Loop 2 is written as

$$\phi_2 = \int \vec{B}_1 d\vec{a}_2 \tag{44}$$

Since $\vec{B}_1$ is proportional to the current I_1, we may define the mutual inductance as the constant of proportionality between the flux ϕ_2 and the current I_1 as

$$\phi_2 = M_{1,2} I_1$$

The magnetic field can be written in terms of the vector potential accordingly to Equation 5. By doing that and also by invoking Stokes' theorem we may rewrite Equation 44 as

$$\phi_2 = \int \left(\vec{\nabla} x \vec{A}_1\right).d\vec{a}_2 = \oint \vec{A}_1.d\vec{s}_2 \tag{45}$$

On Equation 45 the element of length $d\vec{s}_2$ strings along the wire path of Loop 2. Now the vector potential can be calculated through the use of Equation 23, without the homogeneous contribution. Here, we will consider that the two current loops are close to each other, so that retardation effects can be neglected. Also, there is no incoming electromagnetic radiation, and the homogeneous solution can be discarded. By putting retardation effects aside and also by integrating along the cross sectional area of the wire, the vector potential $\vec{A}_1$ can be obtained from:

$$\vec{A}_1(\vec{r}) = \frac{\mu_o I_1}{4\pi} \oint \frac{d\vec{s}_1}{|\vec{r} - \vec{r}\,'|}$$

With this result the flux ϕ_2 on Equation 45 is given by

$$\phi_2 = \frac{\mu_o I_1}{4\pi} \oint \oint \frac{d\vec{s}_1.d\vec{s}_2}{|\vec{r} - \vec{r}\,'|}$$

Finally, the mutual inductance of this couple of loops can be written as

$$M_{1,2} = \frac{\mu_o}{4\pi} \oint \oint \frac{d\vec{s}_1.d\vec{s}_2}{|\vec{r} - \vec{r}\,'|} \tag{46}$$

It is clear from this reasoning that the mutual inductances $M_{1,2}$ and $M_{2,1}$ must be equal since both loops were treated on equal footings. Equation 46 depends on the geometrical properties of the loop paths and also on their relative position. This result is due to Newmann and is frequently known as Newmann's formula.

Although Equation 46 was constructed to obtain the mutual inductance of a pair of current loops, it can also be useful in determining the self inductance of a single loop. In order to do that, the two current loops can be made much alike each other and put in the same spatial location so that, in the limiting case, they converge to just one single loop. The problem with that approach is that the integral may have not be defined anymore in the points where $\vec{r} = \vec{r}\,'$. Nevertheless, consider a conductor of finite cross sectional area like that of Figure 9.a, which posses a wire radius equal to a.

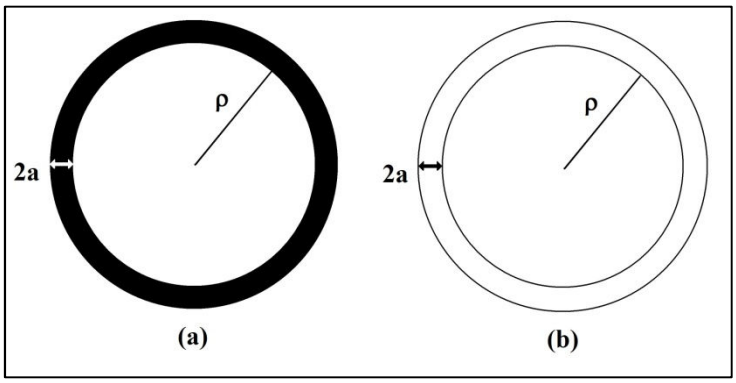

Figure 9: Current loops. (a) Conductor with loop radius equal to ρ and wire radius equal to a. (b) Two filamentary current loops of loop radius equal to ρ and separation equal to a.

The external contribution to the self inductance of this conductor can be obtained by considering two filamentary current loops separated by a distance equal to $2a$, like those of Figure 9.b. This approximation will be reasonable if the wire radius is much smaller than the loop radius, that is, if $a << \rho$. On Figure 9 we draw circular loops for simplicity but the reasoning presented here is valid for any desired wire shape.

2.5.9-Electromagnetics of circuits and radiation resistance

A useful approach in dealing with the electromagnetic fields on electrical circuits is to separate the electric field into an applied and an induced portion. Although artificial, this separation may turn the analysis easier. The applied portion is defined as

that which is built due to the presence of the applied potential difference only. The induced portion is that part of the electric field which is generated from the dynamics of the electrical charges and currents which may be present as consequence of the applied potential. This way, we write the electric field ($\vec{E}$) as the sum of the applied ($\vec{E}_o$) and the induced ($\vec{E}'$) fields. It is useful to write the induced part in terms of the electromagnetic potentials, once the latter can be easily obtained from the charges and currents in the circuit, through the use of Equations 22 and 23. This results in:

$$\vec{E} = \vec{E}_o + \vec{E}' = \vec{E}_o - \frac{\partial \vec{A}}{\partial t} = \frac{\vec{J}}{\sigma} \tag{47}$$

On the last step of Equation 47 the Ohm's law was used. If however there are parts of the circuit which are non-conducting, the association of the electric field to a current density is not well defined there. For those regions both $\vec{J}$ and σ are null.

Figure 10 below illustrates a circuit path being fed by a generator. The potential difference varies harmonically in time, and an instantaneous potential difference V_o is shown:

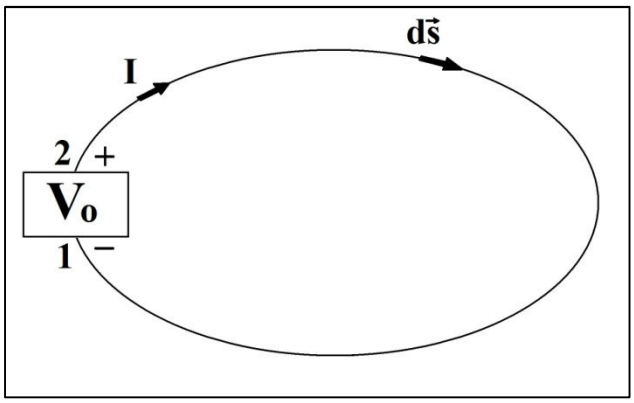

Figure 10: Circuit path being fed by a generator.

If the fields on Equation 47 are integrated along the entire circuit length, the following result is obtained:

$$\int_1^2 \vec{E}_o.d\vec{s} - \int_2^1 \frac{\partial \vec{A}}{\partial t}.d\vec{s} - \int_2^1 \frac{\vec{J}}{\sigma}.d\vec{s} = 0 \tag{48}$$

The first integral on Equation 48 is readily recognized as the potential difference introduced by the generator in the circuit, as defined by:

$$V_o = \oint \vec{E}_o.d\vec{s} = \int_{2\ circuit}^{1} \vec{E}.d\vec{s} = -\int_{1\ generator}^{2} \vec{E}_o.d\vec{s}$$

The harmonic time dependence on the above equation was omitted for simplicity. The last integral on Equation 48 was already computed for a particular case in subsection 2.5.1 by working with the resistance effect. There we have assumed a constant conductivity, but that is not a limiting constraint because a position dependent conductivity can be easily integrated along the circuit path. We have also assumed that the current is equally independent of position. This last restriction was necessary in order to guarantee the electrical charge conservation from the point of view of electrostatic or *quasistatic* situations.

With these results, and also by recalling the harmonic time dependence which was assumed to be present in the excitation signal from the generator, Equation 48 is rewritten as

$$V_o - Z_{\text{int}} I - i\omega \oint \vec{A}.d\vec{s} = 0 \tag{49}$$

On Equation 49 we have defined the internal impedance of the circuit path as the part of the impedance apart from the contribution of the vector potential. For low frequency values it can be associated with the resistance of the wire which was deduced on subsection 2.5.1, and for higher frequency values it can be associated with the Skin impedance defined on subsection 2.5.6.

In order to obtain the whole impedance expression for the closed circuit path of Figure 10, the vector potential is demanded. Equation 23 is a general expression which gives the vector potential as function of the current density. It can be simplified by integrating the current density along the cross sectional area of the wire. Since there is no incoming electromagnetic radiation, the homogeneous solution can be discarded. If the distribution of the current along the wire radius in unimportant, that is, if this circuit is treated as having a filamentary current, we have:

$$\vec{A}(\vec{r},t) = \frac{\mu_o}{4\pi} \oint \frac{I_{ret}}{|\vec{r} - \vec{r}\,'|} ds' = \frac{\mu_o I}{4\pi} \oint \frac{\exp\left[i\omega \left(t - \frac{|\vec{r} - \vec{r}\,'|}{c} \right) \right]}{|\vec{r} - \vec{r}\,'|} d\vec{s}\,' \tag{50}$$

On the last equation s' strings along the entire wire length and $\vec{r}\,'$ localizes the current element. By assuming a filamentary current we consistently neglect the Skin impedance, since the distribution of current inside the wire is assumed to be constant. The internal impedance in this case is simply given by the resistance of the wire, and Equation 49 can be rewritten as:

$$V_o - RI - i\omega \frac{\mu_o I}{4\pi} \oint\oint \frac{\exp\left(-ik\,|\vec{r}-\vec{r}\,'|\right)}{|\vec{r}-\vec{r}\,'|} d\vec{s}.d\vec{s}\,' = 0 \tag{51}$$

The harmonic temporal dependence was also omitted on Equation 51, and the parameter $k = \omega / c$ has the same definition as that given by Equation 13.

The impedance of the circuit is then readily expressed as the ratio between applied potential difference and resulting current as:

$$Z(\omega) = \frac{V_o}{I} = R + i\omega \frac{\mu_o}{4\pi} \oint\oint \frac{\exp\left(-ik\,|\vec{r}-\vec{r}\,'|\right)}{|\vec{r}-\vec{r}\,'|} d\vec{s}.d\vec{s}\,' \tag{52}$$

By expanding the complex exponential on the above integral, we can perceive that, besides the internal impedance, there are two impedance elements. One of them possesses a null phase angle and other presents a phase angle equal to π/2, as defined below:

$$\begin{aligned} Z(\omega) &= R + R_r + i\omega L \\ R_r &\equiv \frac{\omega\mu_o}{4\pi} \oint\oint \frac{\sin(k\,|\vec{r}-\vec{r}\,'|)}{|\vec{r}-\vec{r}\,'|} d\vec{s}.d\vec{s}\,' \\ L &\equiv \frac{\mu_o}{4\pi} \oint\oint \frac{\cos(k\,|\vec{r}-\vec{r}\,'|)}{|\vec{r}-\vec{r}\,'|} d\vec{s}.d\vec{s}\,' \end{aligned} \tag{53}$$

The general impedance formula expressed by Equation 53 contains two terms for which the currents are in phase with the applied voltage. These are the internal impedance of the wire (R), and also another impedance (R_r) which is generally called the radiation resistance and accounts for the energy which is radiated from the circuit. There is also another impedance term (L) with a phase angle equal to π/2, which is a generalization to Newmann's formula expressed on Equation 46. It is straightforward to see that it reduces to Newmann's formula for the low frequency limit by expanding the cosine function on the integral and by keeping only the lowest order term. Higher order terms represent corrections on the inductance of the circuit for higher frequency values.

3-A model for undamped waves on ohmic materials

In Chapter 2 we have presented the most common electromagnetic effects relevant to impedance calculations, as an introductory route to our work. All of the preceding analysis is standard and detailed explanations of it can be readily found on classical textbooks [54-55] of electromagnetism. In this chapter we present novel results concerning the calculation of a yet, unreported impedance. We have theoretically predicted this impedance which posses a negative real part. In an equivalent manner, its phase angle is capable of attaining a value of π.

All of the impedance formulas of Chapter 2 present a positive or null real part. As far as we know, this is assumed to be true for any passive device. This is clearly true for the resistor, the capacitor, and the inductor. The Skin impedance and the Warburg impedance also present non-negative real parts. It is also possible to shown that the radiation resistance defined on Equation 53 is always a positive number. Nevertheless, we argue that the impedance of a passive circuit may still present negative values under specific physical conditions.

3.1-The presence of undamped current waves

In order to construct a model capable of explaining the negative real part impedance, consider a closed loop of conducting material for which a harmonic signal is applied between its extremities, just like that of Figure 10. For the frequency range commonly used on electrical impedance measurements, it is reasonable to assume that no charge density would exist inside a conducting material as consequence of the applied field. The reason for that, as discussed with a little more detail in Chapter 2, is that an electromagnetic field does not easily penetrate the bulk of a good conducting material. Any charges inside it would induce additional redistributing charges in a way to neutralize the initial distribution in a very fast manner due to the extraordinarily high mobilities of the charge carries. For these reasons, Equation 10 which permitted us to obtain the electrical potential as function of the electrical charge density is rewritten as:

$$\nabla^2 V + \frac{\omega^2}{c^2} V = 0 \tag{54}$$

Equation 54 is commonly used to treat the case of a transmission line [55]. The circuits which we shall consider here are small enough in such a way that transmission line effects are not relevant. Nevertheless, Equation 54 will still be used in order to obtain the electrical potential along the circuit path. For a long conductor, meaning its length much larger than its typical diameter, Equation 54 admits solutions comprising longitudinal undamped propagating modes of the form: $V \sim e^{\pm iks}$, where $k = \omega / c$. Here, s is a coordinate that strings along the wire length as usually made in Chapter 2. This approximation is reasonable for the case of large spires, meaning their curvature radius is much larger in comparison with the typical wire diameter. Given that the excitation potential difference is applied across the wire axis, the boundary conditions for a wire of total length l, and grounded at $s = 0$, is $V(s=0) = 0$ and $V(s=l) = V_o \exp(i\omega t)$.

In view of that, the applied electric field would also present longitudinal modes. Moreover, for an ohmic material the current density is proportional to the applied electric field and would present this way, longitudinal modes as well. That is, we assume a current density of the kind

$$\vec{J}_s = J_o e^{+i(\omega t + ks)} \hat{s} \tag{55}$$

The positive sign in the exponent is consistent with the boundary conditions, in which the active pole of the source is at the end of the wire length ($s = l$). That is, the phase velocity directs to the ground.

Equation 55 expresses a non-trivial hypothesis which shall be used for the rest of this chapter in deriving our theoretical model. For this reason, we make a pause in the theoretical development in order to show some experimental evidence for these current waves. With this, we hope to provide some degree of soundness to our initial assumption. Detailed experimental results will be presented in Chapter 4.

In order to directly observe these waves on a wire, we have made an experiment comprising a coil and a RF generator directly connected to it. An oscilloscope was used to monitor the Root Mean Square (rms) potential difference between the generator's ground (one of the coil extremities) and various points along the coil wiring. Experimental details and instrument specifications are provided on section 4.5 (Oscilloscope measurements). Choosing to make this measurement on a coil instead of a single spire was a matter of simplicity. This is because a large wire length is necessary to observe the modulating current phenomenon at frequency values which are not too

high. Also, measuring the potential along the length of a large spire would require large connecting cables presenting considerable impedances, and disturbing the measurement in a non trivial way. This way, the compact topology of a coil was appropriate for this investigation. A scheme of this experimental setup is shown on Figure 11 below:

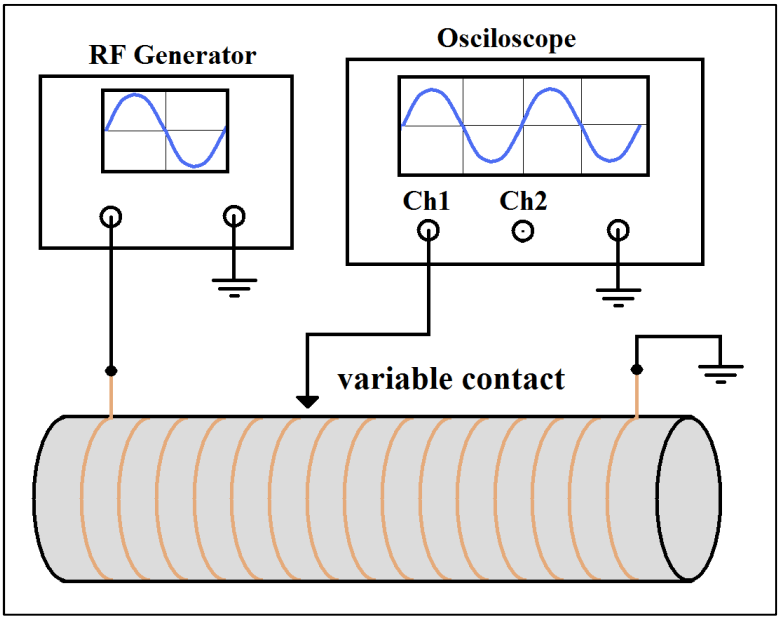

Figure 11: Scheme of the experimental setup for potential difference measurements along the length of the conductor, using an oscilloscope.

As can be seen of Figure 11, by using a variable contact the measurement of the potential difference between several points of the coil was possible. A coil possessing 100mm of diameter was constructed from a 100μm diameter constantan* wire with an inter-spire separation of 8mm, and a total of 44 turns which gives a total wire length of about 14m. This coil was connected to a RF generator and the frequencies of 1MHz, 10MHz, 20MHz and 40MHz were applied. An oscilloscope reads the rms potential difference between the ground and various points along the wire length. Normalized oscilloscope readings as function of the position of the variable contact are displayed on Figure 12:

* Constantan is a copper-nickel alloy. It is consisted of approximately 55% of copper and 45% of nickel. The conductivity of this material is fairly constant over a wide range of temperatures.

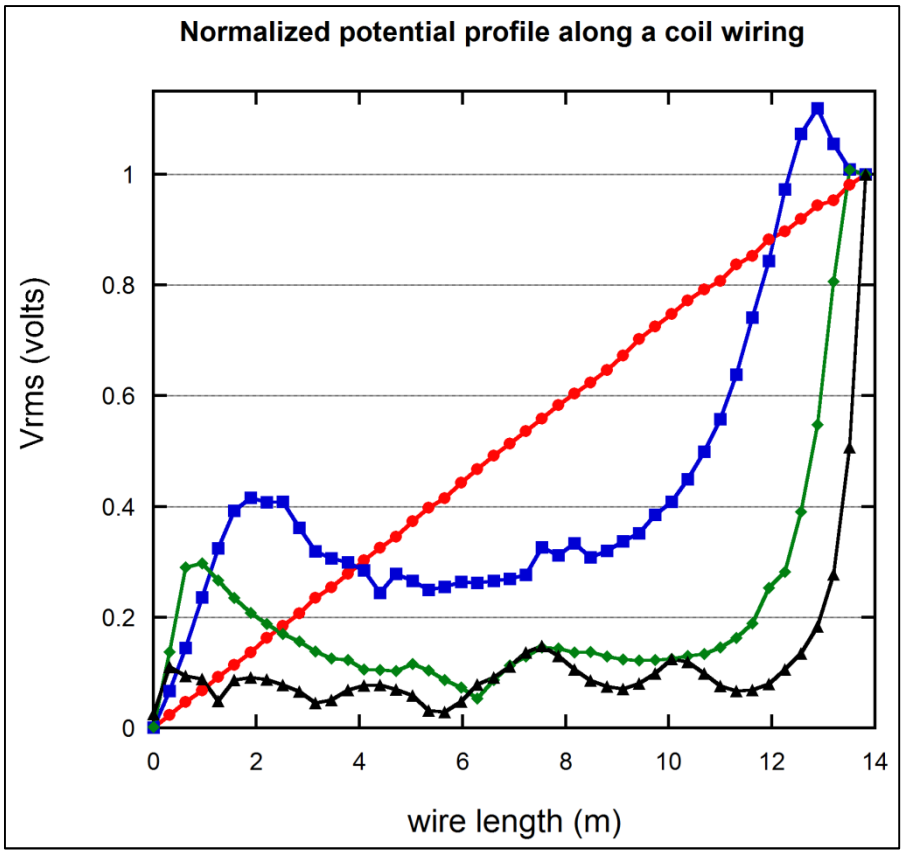

Figure 12: Normalized potential profile along the constantan coil wiring. Root mean square potential difference between the ground and several points along the length of a constantan coil at several frequencies: 1MHz (●), 10MHz (■), 20MHz (♦) and 40MHz (▲).

As can be checked in the 1MHz curve, the expected linear drop for the electrical potential along the wire is confirmed, evidencing a constant electric field at low frequencies. For higher frequencies the electrical potential displays a strong deviation from linearity. Near the generator's active pole (great distances from the ground) it is observed a large applied electric field. For distances to the ground smaller than 10m, a modulated stream of data superimposed upon an almost constant potential profile is observed. The modulation is clearly visible at 40MHz. This effect suggests the existence of a nontrivial dynamics for the electromagnetic field on the wire.

The preceding analysis suffices to infer the presence of a non homogeneous current density in the wire. This way we have enough justification for the use of a spatially-dependent current, as that given by Equation 55.

3.2-The general impedance formula for a single spire

The spatially modulated current density expressed by Equation 55 generates a vector potential responsible for induced magnetic and electric fields in and around the wire. The electromotive force generated this way is just a time derivative of the (retarded) vector potential integrated along the wire path. This will lead to an impedance expression that is a proper generalization of the Neumann's formula. As will be shown, the presence of undamped spatial modes along the wire axis would produce, at specific frequency ranges, a current density at the source which is in counter phase with the applied potential. This new reactive effect is the cause of the observed negative real part impedance. It must be stressed that usual ohmic dissipation is still present for all frequencies since the internal impedance of the wire is always present, but it may be overcome by the reactance we observed. As a result, the impedance phasor angle runs over the full trigonometric circle.

In order to obtain a general formula for the impedance of a single spire we may reconsider the developments from Equation 48 through Equation 52 again. There we have integrated the electric field along the circuit path in order to obtain the potential drops along the circuit as function of the current. The difference in our approach this time is the relaxation of the homogeneous current constrain. A homogeneous current is necessary in the context of electrostatics, for it represents the principle of electrical charge conservation in that situation. For non stationary fields however, it may be an oversimplification of the problem as pointed out on section 3.1. Still, a homogeneous current is frequently assumed in many impedance calculations, as for example in Newmann's formula, expressed here by Equation 46.

Then, by considering the spatially modulated current density of Equation 55 we may recast the vector potential of Equation 50 by making the following adjustment: $I \to I\exp\left[ks(\vec{r}\,')\right]$. This results in:

$$\vec{A}(\vec{r},t)=\frac{\mu_o}{4\pi}\oint\frac{I_{ret}}{|\vec{r}-\vec{r}\,'|}ds'=\frac{\mu_o I}{4\pi}\oint\frac{\exp\left[i\left(\omega t+ks(\vec{r}\,')-\frac{\omega|\vec{r}-\vec{r}\,'|}{c}\right)\right]}{|\vec{r}-\vec{r}\,'|}d\vec{s}\,' \quad (56)$$

On the Equation 56 the integration of the current density along the cross sectional area of the wire was already performed. Thus we may rewrite Equation 51 as:

$$V_o - RI - i\omega \frac{\mu_o I}{4\pi} \oint\oint \frac{\exp\left[ik\left(s(\vec{r}\,') - |\vec{r} - \vec{r}\,'|\right)\right]}{|\vec{r} - \vec{r}\,'|} d\vec{s}.d\vec{s}\,' = 0 \qquad (56)$$

Circuit impedance is then defined as the ratio of the source potential difference to the current. Its expression is analogous to Equation 52, and is given by

$$Z(\omega) = \frac{V_o}{I} = R + \frac{i\omega\mu}{4\pi} \oint\oint \frac{\exp\left[ik\left(s(\vec{r}\,') - |\vec{r} - \vec{r}\,'|\right)\right]}{|\vec{r} - \vec{r}\,'|} d\vec{s}.d\vec{s}\,' \qquad (57)$$

The result expressed by Equation 57 is different from that one usually employed to get radiation resistance because of the presence of the spatially modulated current. Existence of a non-homogenous current distribution leads to a complex-valued result for the integral. Its real part is just a generalization of circuit inductance. Its imaginary part, not present under a homogenous current distribution, represents a new circuit effect. The integral in Equation 57 can be viewed as representing a complex inductance (that is an inductance presenting both real and imaginary parts) and clearly describes a reactive effect. The imaginary part of this generalized inductance produces a negative real part contribution for the circuit impedance.

3.3-Numerical evaluations for the impedance of a spire

The result of the last section permits us to easily perform numerical evaluations, once a closed and analytical expression for the impedance was retrieved. Still, the integrand of Equation 57 is dominated by the singularity at $\vec{r} = \vec{r}\,'$, and a regularization procedure must be performed. The singularity of the integral may be removed by rewriting the denominator on the integrand as:

$$|\vec{r} - \vec{r}\,'| \to \sqrt{\left(\vec{r} - \vec{r}\,'\right)^2 + \phi^2}$$

We have performed calculations for a round conductor by choosing a value for ϕ, which is equal to the wire diameter. This approximation is consistent with the reasoning of subsection 2.5.8, in which the self inductance of a spire was computed by using the mutual inductance of two nearby spires of same shape. By excluding the region within the wire from the integral, we give only the external contribution for the generalized inductance. This approximation is reasonable for the case of a filamentary current, that is, if the spire typical dimensions are much greater than wire radius.

In order to consistently check the result of Equation 57 against one of our experiments, numerical data was obtained for a rectangular spire. The structure of Equation 57 demands a double integration along the wire path. The case of a rectangular spire is easy to compute because the length elements are either in the same direction or are perpendicular to each other. Then we need to consider only those situations for which they are parallel: $d\vec{s}.d\vec{s}' = dsds'$ and also those situations for which they are anti-parallel: $d\vec{s}.d\vec{s}' = -dsds'$. For the cases in which the length elements are perpendicular we have: $d\vec{s}.d\vec{s}' = 0$. Figure 13 below illustrates this spire and the geometrical considerations which we have used:

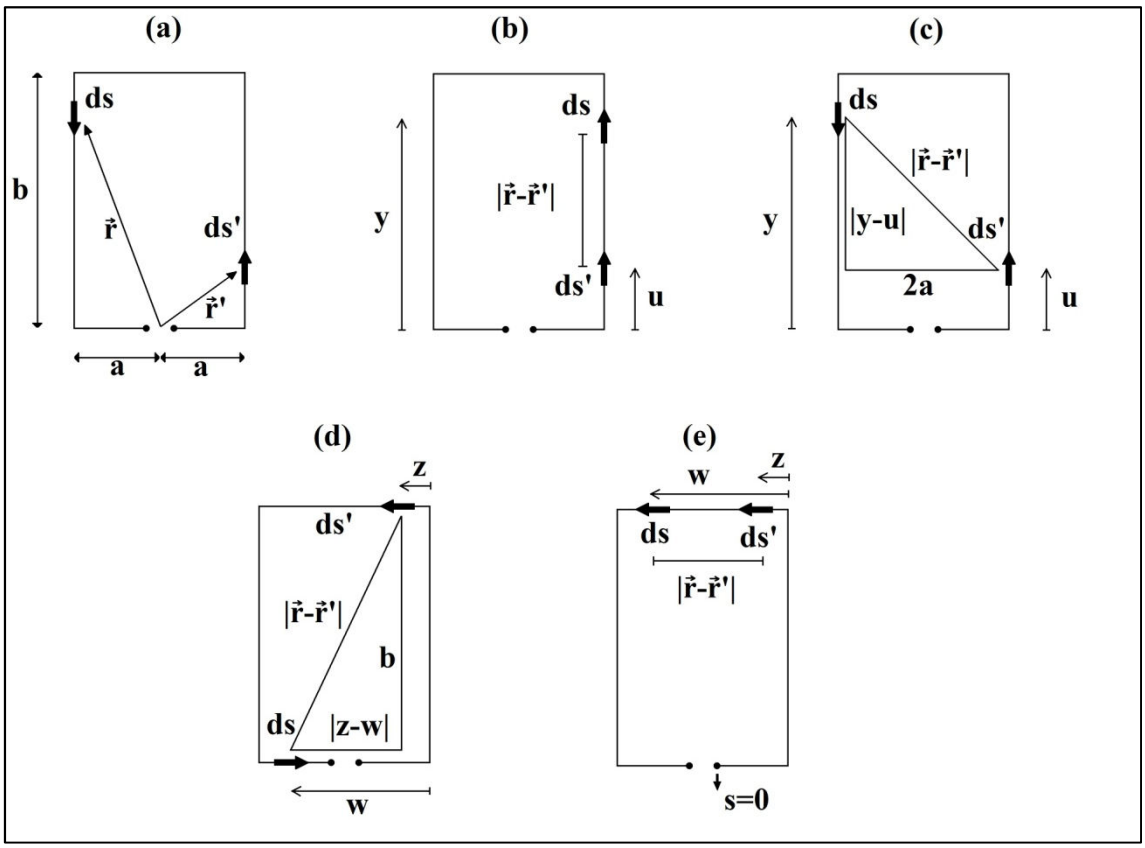

Figure 13: Geometry of the rectangular spire. (a) Spire dimensions and definition of the length elements. (b) Case in which ds and ds' are both on the same side, along the greater dimension. (c) Case in which ds and ds' are one at each of the greater dimension sides. (d) Case in which ds and ds' are each at one of the smaller dimension sides. (e) Case in which ds and ds' are both on the same side, along the smaller dimension.

In view of the scheme presented on Figure 13, it is possible to break up the double closed path integral into some simpler integrals, involving only one segment of the circuit at each time. In order to compare our calculations with one of our experiments,

we have considered a rectangular spire as made of a round copper wire having a diameter equal to $\phi = 55\mu m$, and with the following spire dimensions: $a = 15cm$ and $b = 11,08m$. This results in a total wire length of approximately 23m and a spire width of 30cm.

Wire resistance was calculated using Equation 26 and copper electrical conductivity at room temperature $\sigma = 5.96 \times 10^7 \Omega^{-1} m^{-1}$. Thus Equation 57 was numerically computed by the following expression:

$$
\begin{aligned}
Z(\omega) = {} & \frac{8(a+b)}{\sigma\pi\phi^2} + \frac{i\omega\mu}{4\pi}\left[\int_0^b\int_0^b \frac{\exp\left[ik\left(s1(u)-|y-u|\right)\right]}{\sqrt{(y-u)^2+\phi^2}}dydu + \int_b^0\int_b^0 \frac{\exp\left[ik\left(s2(u)-|y-u|\right)\right]}{\sqrt{(y-u)^2+\phi^2}}dydu\right. \\
& -\int_0^b\int_b^0 \frac{\exp\left[ik\left(s1(u)-\sqrt{(2a)^2+(y-u)^2}\right)\right]}{\sqrt{(2a)^2+(y-u)^2}}dydu - \int_b^0\int_0^b \frac{\exp\left[ik\left(s2(u)-\sqrt{(2a)^2+(y-u)^2}\right)\right]}{\sqrt{(2a)^2+(y-u)^2}}dydu \\
& -\int_{2a}^0\int_0^{2a} \frac{\exp\left[ik\left(s3(z)-\sqrt{b^2+(z-w)^2}\right)\right]}{\sqrt{b^2+(z-w)^2}}dzdw + \int_0^{2a}\int_0^{2a} \frac{\exp\left[ik\left(s3(z)-|z-w|\right)\right]}{\sqrt{(z-w)^2+\phi^2}}dzdw \\
& -\int_0^{2a}\int_a^0 \frac{\exp\left[ik\left(s4(z)-\sqrt{b^2+(z-w)^2}\right)\right]}{\sqrt{b^2+(z-w)^2}}dzdw - \int_0^{2a}\int_a^0 \frac{\exp\left[ik\left(s5(z)-\sqrt{b^2+(z-w)^2}\right)\right]}{\sqrt{b^2+(z-w)^2}}dzdw \\
& \left. +\int_{2a}^0\int_{2a}^a \frac{\exp\left[ik\left(s6(z)-|z-w|\right)\right]}{\sqrt{(z-w)^2+\phi^2}}dzdw + \int_{2a}^0\int_a^0 \frac{\exp\left[ik\left(s5(z)-|z-w|\right)\right]}{\sqrt{(z-w)^2+\phi^2}}dzdw\right]
\end{aligned}
\tag{58}
$$

On the numerical expression given by Equation 58, the following functions were used in order to specify the $s(\vec{r}\,')$ term:

$$s1(u) = a + u \;\; ; \;\; s2(u) = 3a + 2b - u \;\; ; \;\; \text{s3(z)=a+b+z}$$

$$\text{s4(z)=4a+2b-z} \;\; ; \;\; \text{s5(z)=a-z} \;\; ; \;\; \text{s6(z)=5a+2b-z}$$

Calculated and experimental data are presented on Figure 14 below:

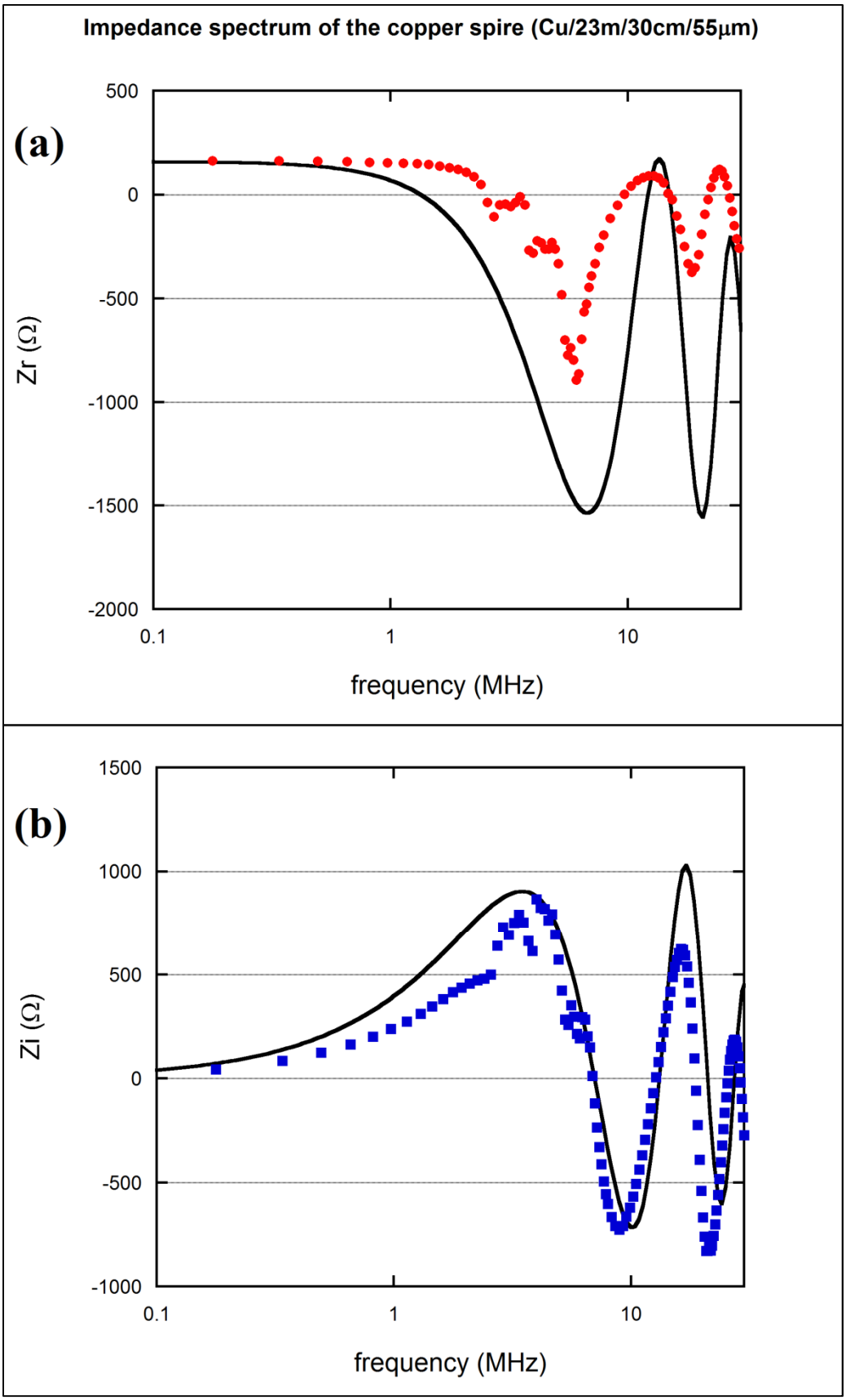

Figure 14: Impedance spectrum of the copper spire (Cu/23m/300mm/55μm): theory (solid lines) and experiment (symbols). (a) Real part impedance spectrum. (b) Imaginary part impedance spectrum.

We can check on this figure that both the real part (Figure 14.a) as well as the imaginary part (Figure 14.b) of the impedance attains positive and negative values. It is clear from this figure that the imaginary part of the impedance was reproduced with good agreement while the real part impedance presented deviations which will be commented in detail on the next chapter.

In what follows we give a detailed description of all experiments that we have made, including the impedance measurement of the copper spire which was presented in advance along with the theoretical calculations on Figure 14.

4-Measurements and experimental data

In this chapter we describe in detail the arrangement of our experiments. Essentially, we measured the impedance of a set of spires and coils of particular geometry avoiding as much as possible circuit artifacts, like inductances and capacitances generated by the connection cables or ground impedances. In order to guarantee that no external sources could interfere in our experiment, metallic shields were constructed and enclosed some of our circuits. Also, it was possible to visualize the applied signal and resulting current on our passive circuits presenting a phase difference of π, on an oscilloscope screen.

4.1-Direct impedance measurements

Direct impedance measurements were performed on both, single spires and coils. For this purpose we made use of a Novocontrol Alpha-A High Performance Frequency Analyzer Impedancemeter. It has a 10TΩ input resistance in parallel with a 0.5 pF input capacitance. Its frequency range spans the μHz to 40MHz interval. Measurements were performed in the frequency range of 10kHz to 35MHz and with an excitation amplitude ranging from 10 to 1000mV. Homemade data acquisition software was used to control the impedancemeter via a standard GPIB interface card. Since we are concerned with a until now forbidden spectrum part, the utilization of commercial software was avoided because it may destroy the correct information on raw data through the use of measurement error control techniques.

The principles of operation of this impedancemeter are those already discussed on section 2.3. In this case, a sine wave is digitally synthesized and applied to a sample as illustrated on Figure 15:

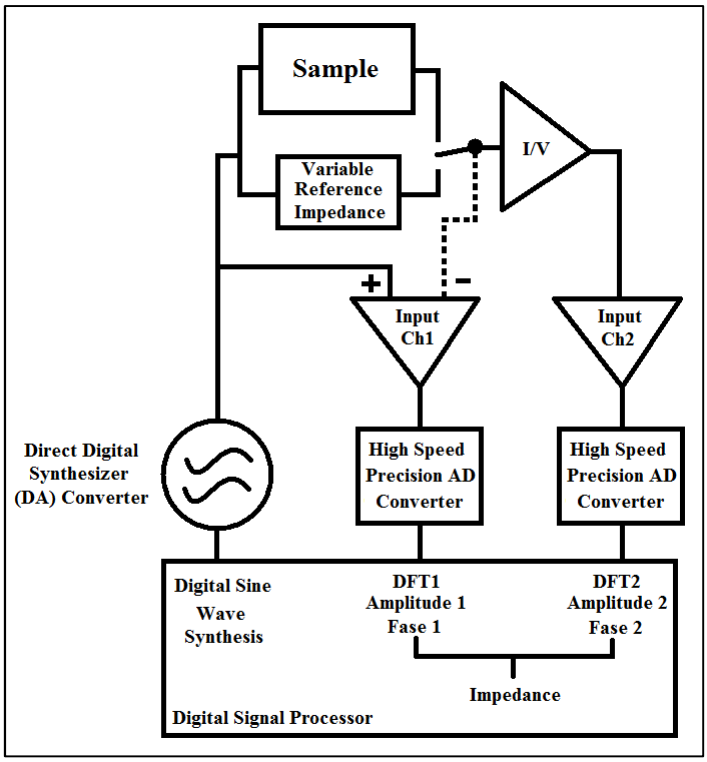

Figure 15: Scheme of impedance measuring method for Novo-Control imipedancemeter.

This is done by a digital signal processor and a high speed digital to analogue converter. This kind of signal generation guarantees high stability and high frequency resolution. Low pass filters are commonly employed to remove some noise that could be generated by the steepness of the digitally created signal. Channel 1 measures the voltage V1 that is applied to the sample. The resulting sample current I_s, is transformed in a voltage V2 by a wide current – wide frequency range precision impedance converter (I/V), and measured by Channel 2. The voltages from these two independent channels are amplified, filtered and converted into two digital data streams. These are phase sensitive and are digitally analyzed with respect to their harmonic base waves by Discrete Fourier Transform (DFT). The ratio between the amplitudes V1 and V2 provides the modulus of the impedance as stated by Equation 4 and the phase angle is simply given by the difference of the phases of those signals.

After each measurement of an impedance point, the sample is replaced by an impedance of reference. The reference measurement includes all linear systematic deviations from the sample and therefore may be used to eliminate them.

The signal processor calculates with a maximum sampling rate of 50MHz, and a resolution of 32bits is attained, corresponding to a step of 10mHz out of 20MHz [56].

In all cases the system under testing was directly plugged to the impedance meter, using the two-wire configuration. Output data consisted of tables comprising the real and imaginary parts as function of the applied frequency.

One of the circuit types we have mounted consisted of large single loop spires. They were constructed using Al, Cu, Ni-Fe alloy and carbon fiber wires. Effects were stronger for larger wire lengths (2 to 26 meters long). Also, it appeared that they must be constructed in a way to avoid large loop inductances (large loop area) and large loop capacitances (small wire separation). These two opposite geometries demanded a careful balance of experimentally adjusted constructive characteristics. Best effects were found for spires built in a rectangular geometry, having 60 to 250mm wire separation. We also observed that the necessary wire length depends on the kind of wire material used. Metallic spires were built with the use of wire diameters ranging from 10 to 1000μm and wire lengths from 4 to 26m. Carbon fiber wires consisted of a bundle of ~5μm fibers forming a 100μm thick sheet. Two types of carbon spires were made. One of them was 4m long and used a 1mm wide sheet. The other was 2m long and used a 2mm wide sheet. In order to properly describe which spire was used on a specific experiment, we adopt the notation: wire material/wire length/wire separation/wire diameter (or width).

The other circuit type consisted of coils directly plugged to the impedancemeter. Coils were made of Al, Cu, brass and constantan wires, wrapped around PVC tubes. These wires had lengths varying between 13 and 25m. However, coil cross sectional area had to be controlled in order to prevent loop inductances which may drive the phase angle to $\pi/2$. The inter-spire capacitance, which may drive the phase angle to $-\pi/2$ at high frequencies, had also to be controlled. This way, the best compromise on wire separation and coil cross-sectional area was empirically determined, avoiding the evidence of strong LC coil impedance. Good results were obtained by use of a coil diameter of 40mm in all experiments. In this sense, spire separation of approximately 1.5mm and 103 to 200 turns was adjusted. Additional cabling necessary to link the coil to the meter was then limited to 100mm (each), introducing negligible extra inductance effects in the measurements. Coils are designed by use of the format material/wire length/wire separation/wire diameter.

4.2-Spire measurements

In this section we report the measurements performed on single spires. Since we observed nontrivial effects in the phase angle (or in the real part impedance) for wire lengths larger than few meters, the balance between spire area and wire separation applies.

In order to test our calculations (Equation 58), a copper spire (Cu/23m/300mm/55μm) was mounted. Its impedance spectrum is shown on Figure 14. It is clearly seen on this figure that the main features of the calculated spectrum were reproduced on both the real (Figure 14.a) and imaginary (Figure 14.b) parts, including the presence of negative real part peaks. The frequencies for which these peaks occurred closely coincide with the corresponding frequencies predicted by the theoretical curve. The depths of the calculated negative real part peaks are considerably larger than the measured ones. Also, measured width for the first negative real part peak is smaller than the theoretically predicted one. This sharper occurrence for the observed minimum in the real part impedance is not trivial and indicates that this model still lacks to explain some of the observed features. This confirms the need for a more precise description of the field dynamics inside the wire. A good agreement between calculated and measured data was obtained for the imaginary part.

Observation of same effects on carbon and Ni-Fe spires demanded less wire length (few meters) whilst other metallic spires were ten or more meters long. For an excitation signal of a few kilohertz the impedance of all spires present, as expected, a characteristic RL response. Moreover, due to skin effects, an additional increase of the impedance as a function of the frequency was also observed. This effect is explicit on the real part data, which displays a consistent increase as function of the frequency. In the Figure 16, we present spectral data for a Ni-Fe spire (Ni-Fe/5.0m/100mm/30μm).

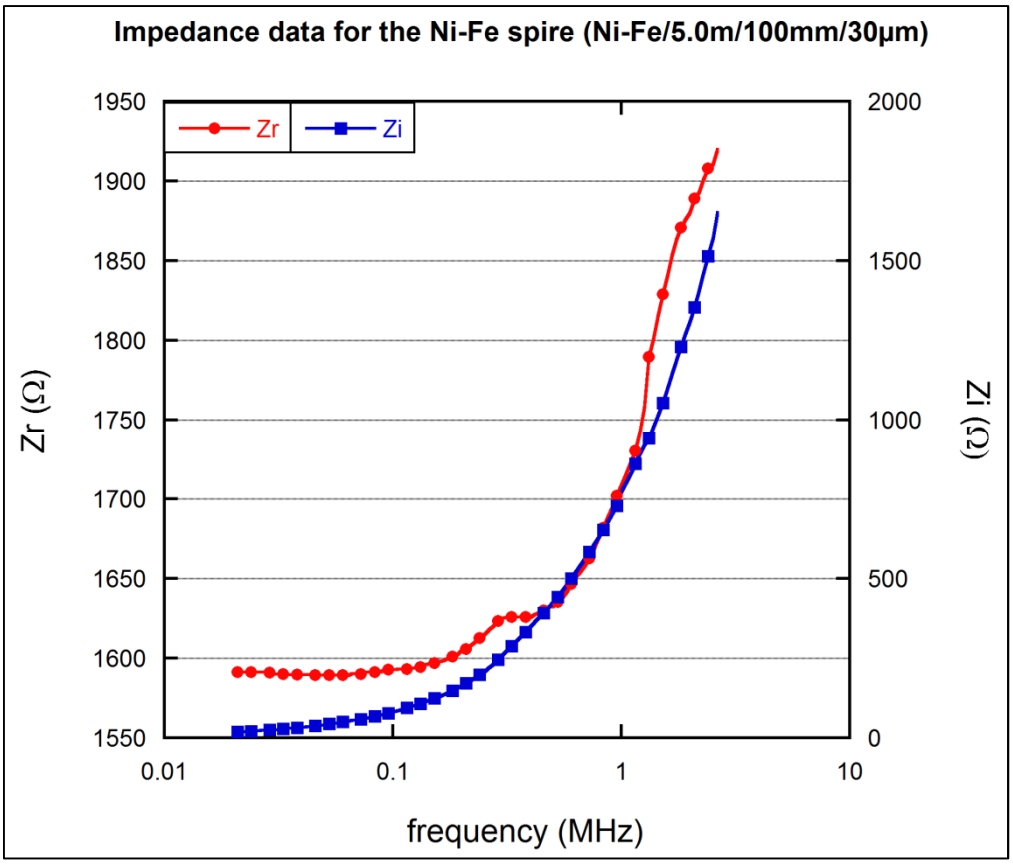

Figure 16: Impedance data for the Ni-Fe spire (Ni-Fe/5.0m/100mm/30µm) covering the frequency interval from 20KHz to 3MHz. On left vertical axis, circles (●) correspond to the real part; while on right vertical axis, squares (■) correspond to the imaginary part.

Due to the strong magnetic susceptibility of this alloy, the skin effect is marked and easily viewed. Note the similarity of this figure with Figure 7 which expresses the impedance per unit length of a 1mm diameter copper wire. However, for frequencies of few megahertz and above, the real part of the impedance of this Ni-Fe spire becomes smaller and assumes negative values. This is shown on Figure 17, where data for the same spire at a larger frequency interval is presented.

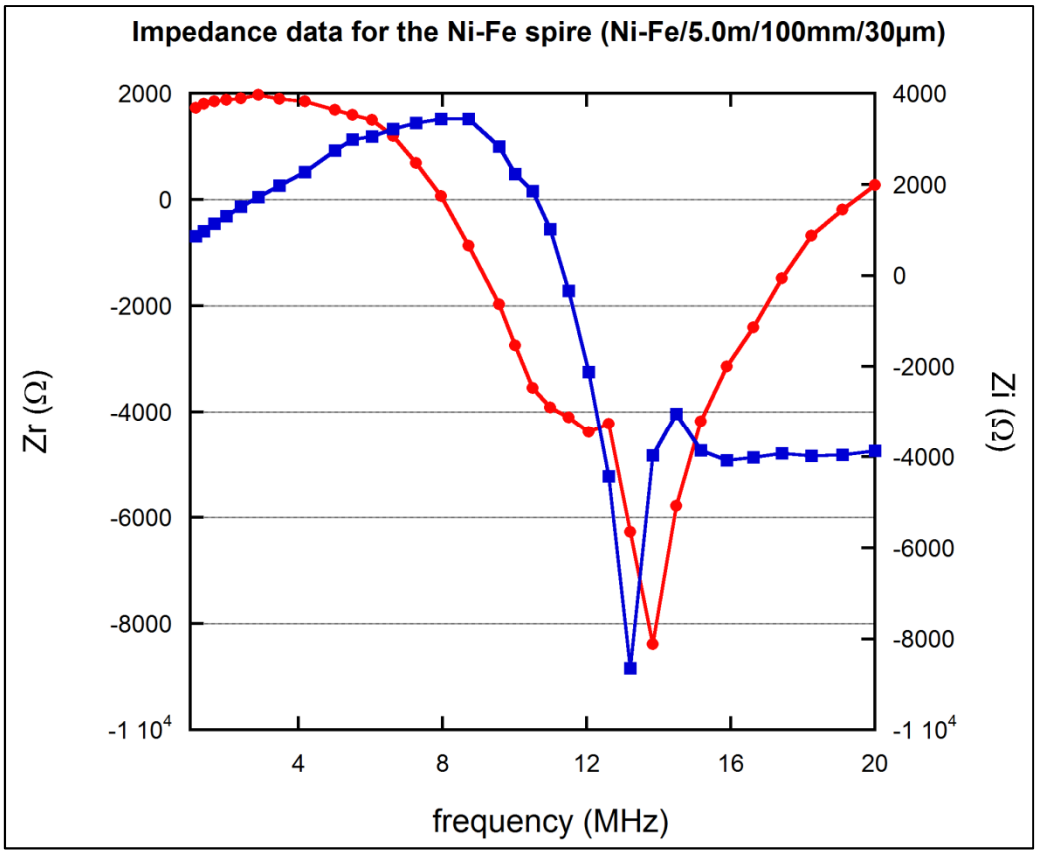

Figure 17: Impedance data for the Ni-Fe spire (Ni-Fe/5.0m/100mm/30µm) covering the frequency interval from 1MHz to 20MHz. On left vertical axis, circles (●) correspond to the real part; while on right vertical axis, squares (■) correspond to the imaginary part.

There, the real part values take a maximum, follow a path to negative values, and reach (at a frequency of 13.8MHz) a minimum of -8.4kΩ. Real part spectra for other spires are presented on Figure 18 below:

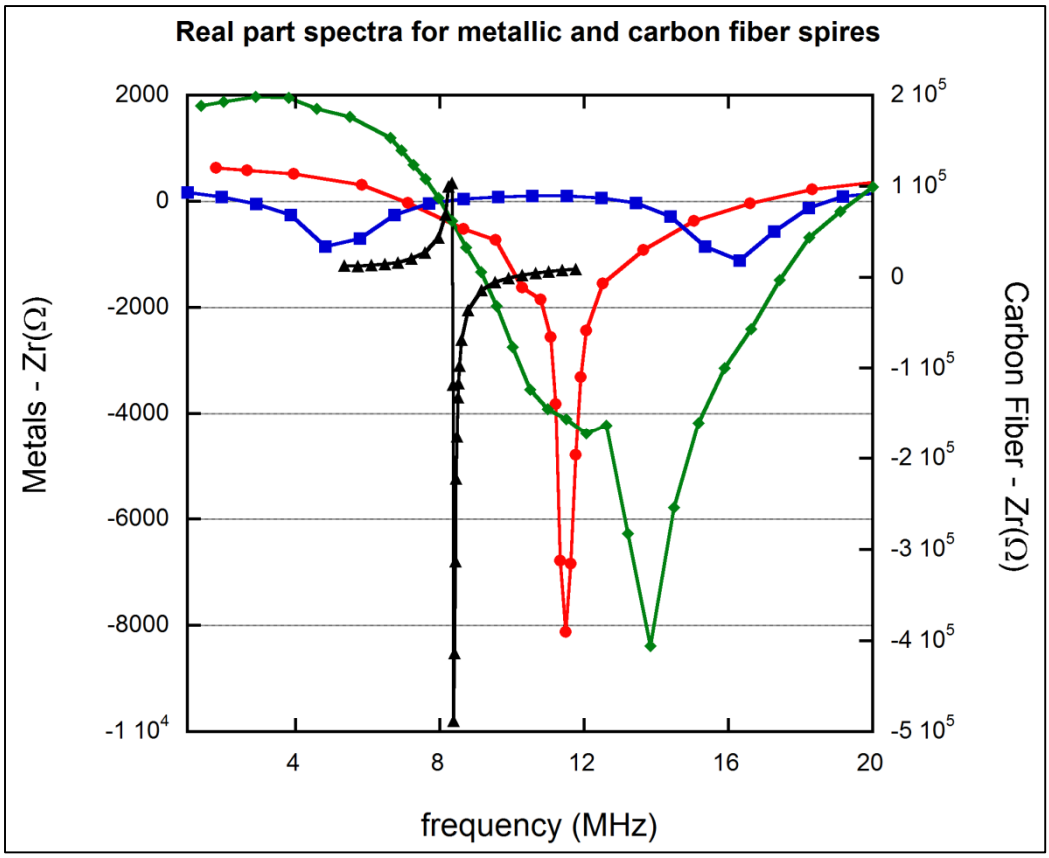

Figure 18: Real part spectra for metallic and carbon fiber spires. On left vertical axis, symbols represent metallic spires data and on right vertical axis, symbols represent carbon fiber spire data. Circles (●) correspond to the aluminum spire (Al/12m/150mm/10µm); squares (■) correspond to the copper spire (Cu/19m/150mm/70 µm); rhombuses (♦) correspond to the Ni-Fe spire (Ni-Fe/5.0m/100mm/30µm) and triangles (▲) correspond to the carbon fiber spire (C/4m/100mm/2mm).

This set of data comprises measurements for spires made of aluminum, copper, Ni-Fe alloy and carbon fiber. Real part profiles are similar to that one shown on Figure 17. The carbon spire (C/4m/100mm/2mm) data (in black) is shown separately on the right vertical axis. Material properties seem to be relevant in this phenomenon. The effect observed using a carbon made spire needed a wire length of only 4m, smaller than those used in all metallic ones. By now we have no reasoning for how material properties can change the value of the negative peak.

Once the real part impedance attains negative values, the phase angle is able to reach the third and fourth quadrants of the trigonometric circle. This effect appears to be more intense for long wires and for small cross-sectional area (dozen microns in diameter), which is consistent with the regularization procedure for the vector potential we have used. This way, a new class of devices and circuits could emerge by use of the extended phase space as presented here. For example, phase modulation circuits could

now explore a larger dynamic range. We provide in Figure 19 the calculated impedance phase angle (from the measured real and imaginary parts) for the carbon spire case.

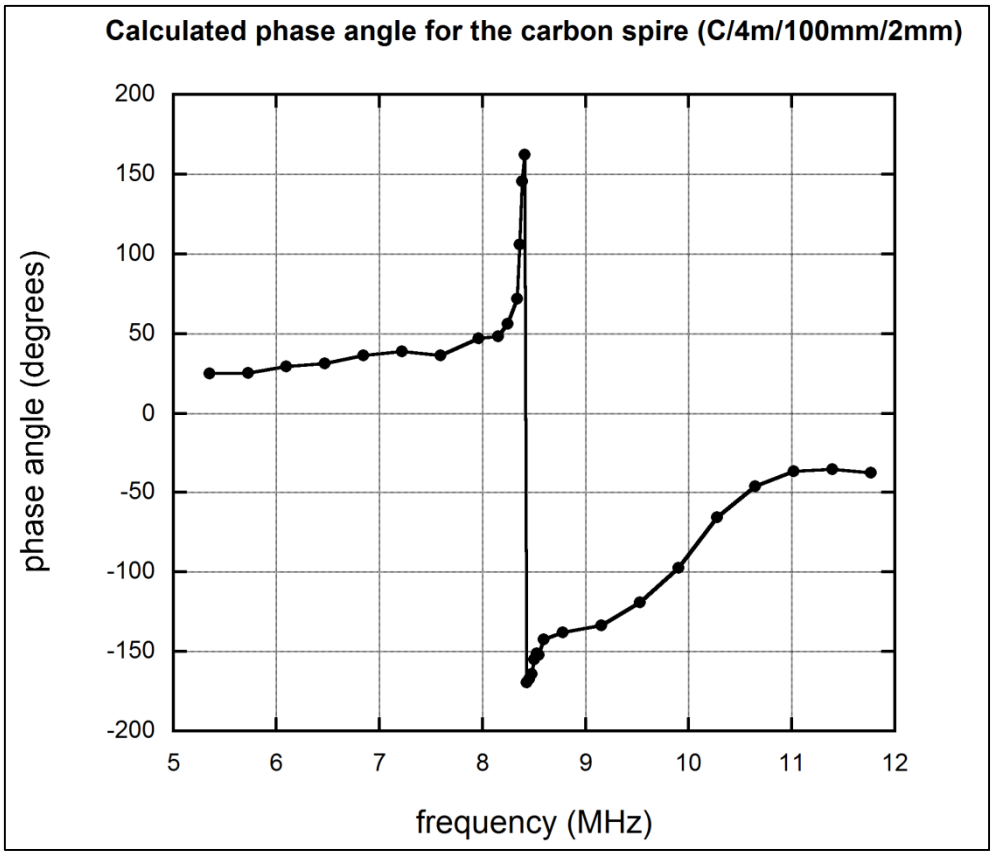

Figure 19: Calculated phase angle for the carbon spire (C/4m/100mm/2mm).

The transition from π to $-\pi$ (a crossing of the negative real axis) is evident. Having passed the resonance, the impedance tends to assume its regular profile, where its real part assumes positive values, comparable to those observed in the low frequency region.

A detailed presentation for the real and imaginary part data is also shown on Figure 20, for another carbon spire (C/2m/100mm/1mm).

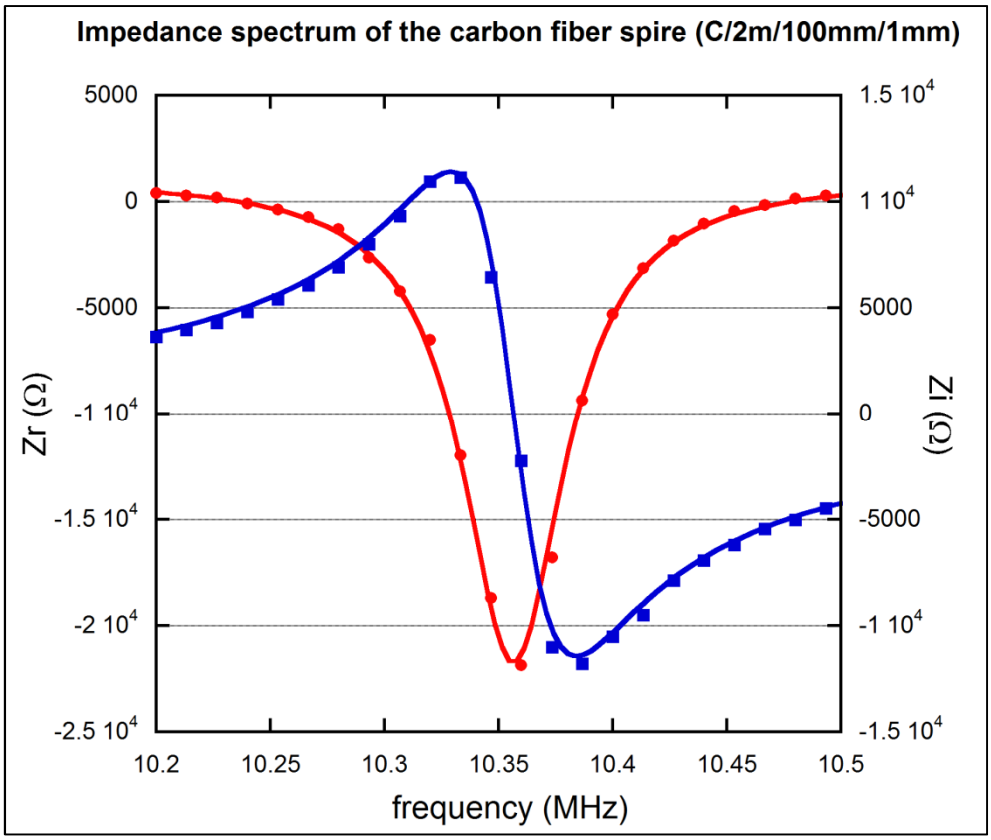

Figure 20: Spectrum of the carbon fiber spire (C/2m/100mm/1mm). On left vertical axis the circles (●) represent the real part; and on right vertical axis the squares (■) represent the imaginary part. Solid lines represent a parallel RLC circuit fitting with a negative resistance value.

Again data present points of extremum in their spectral profile and resemble a kind of resonant peak. In fact, these data (symbols) can be empirically adjusted to a parallel RLC circuit presenting a negative resistance value. In this sense we have adjusted spectral data in the inverted peak region according to the formula:

$$Z(\omega) = R_0 + \left[R^{-1} + i\omega C + (i\omega L)^{-1} \right]^{-1} \tag{59}$$

As shown in Figure 20, the Equation 59 is well suited to the real and imaginary parts of our data. Adjusted parameters are $R_0 = (1.12 \pm 0.07) x 10^3 \Omega$, $R = -(2.29 \pm 0.03) x 10^4 \Omega$, $C = (1.27 \pm 0.02) x 10^{-10} F$ and $L = (1.86 \pm 0.03) x 10^{-6} H$. Differently from an ohmic resistance, where applied electric field and current density vectors are parallel, here they are anti-parallel at the source inputs. As previously shown, this fact is explained as coming from a current density pattern along the wire. This way, the use of these spires as a new circuit element is justified.

Another relevant feature is a qualitative disagreement between the spectral profile of metallic and carbon spires. We have verified that in all metallic spires the imaginary part spectrum, at frequencies close to the inverted peak, reaches its negative minimum first and then rises to a positive maximum. The analogue spectrum for carbon spires initially presents a strong positive spike before its transition to negative values. This behavior is illustrated in Figure 21, which displays the imaginary part spectrum for the aluminum (Al/12m/150mm/10µm) and the carbon (C/4m/100mm/2mm) spire.

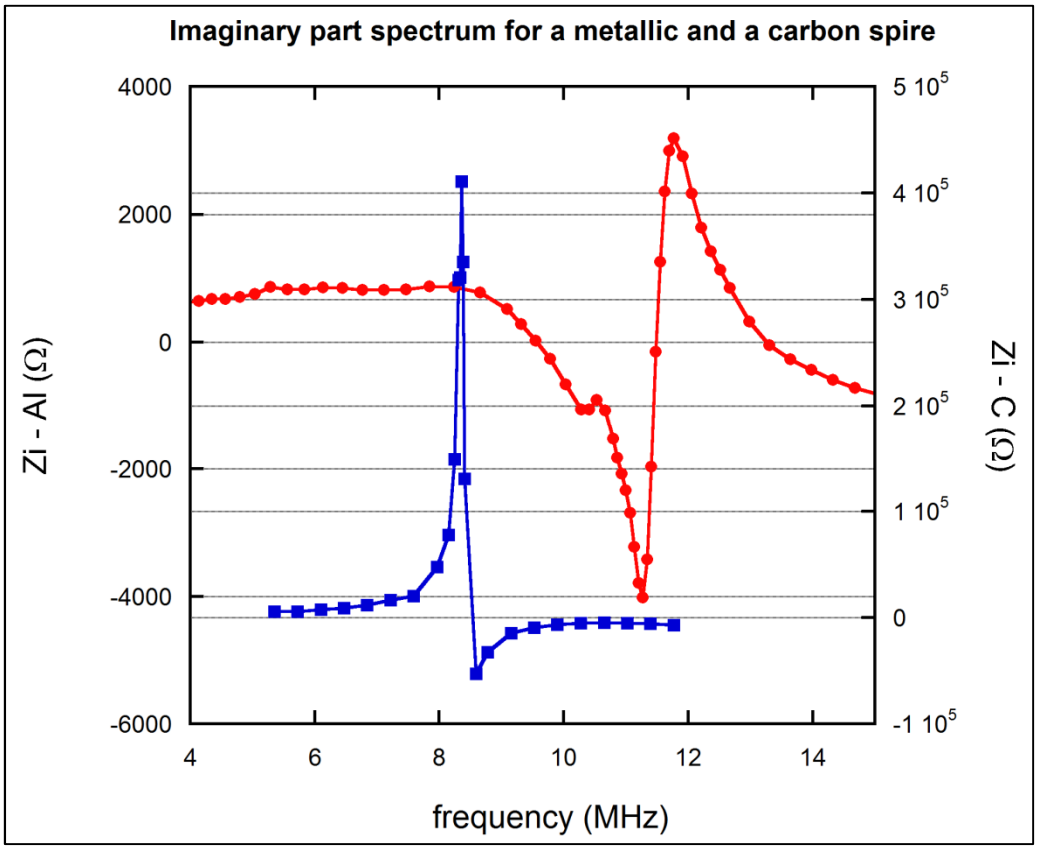

Figure 21: Imaginary part spectrum for a metallic and a carbon spire. On left vertical axis, circles (●) correspond to the aluminum (Al/12m/150mm/10µm) spire data; while on right vertical axis, squares (■) correspond to the carbon (C/4m/100mm/2mm) spire data.

In short, the signal of the derivative at the ZI = 0 point is opposite for metallic and carbon spires.

4.4-Coils measurements

For coils, the challenge of controlling stray effects due to inter-spire capacitance and loop inductance is harder. Since a sufficient wire length is crucial in detecting negative resistance effects, a large number of spires is demanded. Thus a good balance of wire length, inter-spire gap and coil diameter is necessary in order to get the best results. Once again, this compromise was empirically obtained.

The measured spectra for coils are quite different from those observed for single spires, the main difference being the occurrence of multiple inverted peaks in coils. This effect is shown in Figure 22, which presents data for the constantan coil (constantan/27m/1.3mm/100µm).

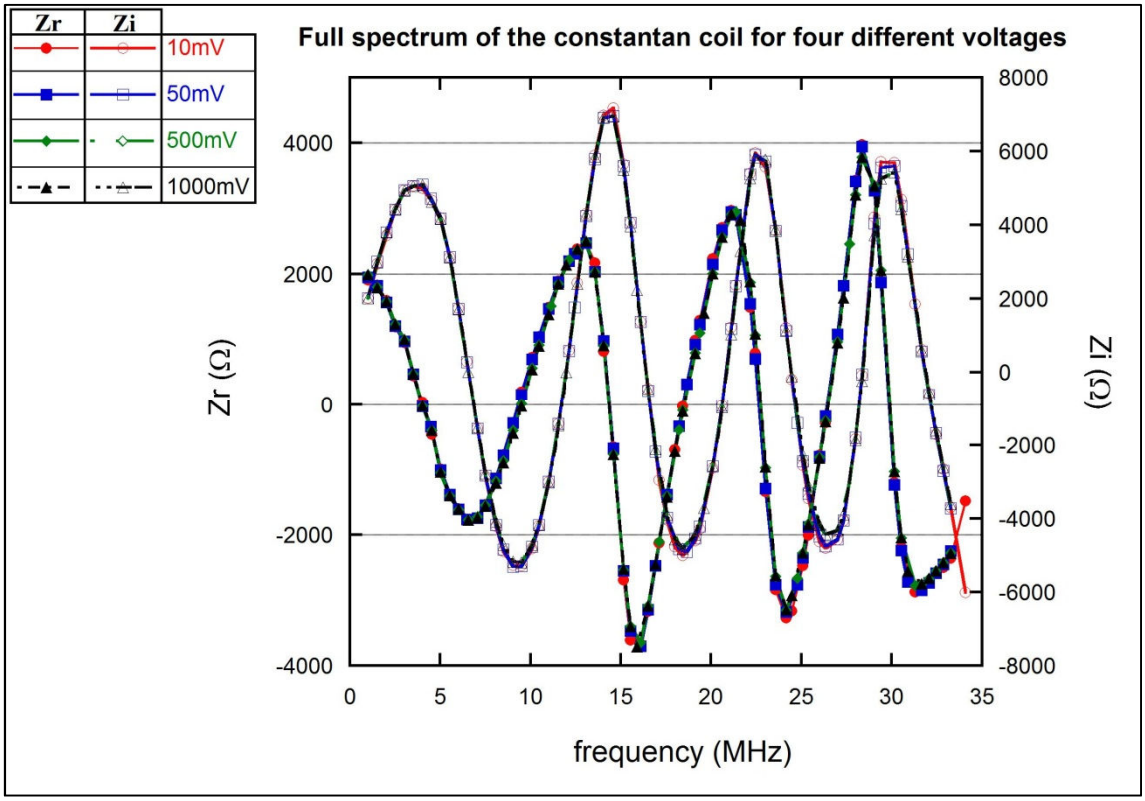

Figure 22: Full spectrum of the constantan coil (constantan/27m/1.3mm/100µm) for four voltages. Full symbols represent the real part and empty symbols represent the imaginary part. Circles (●) correspond to an excitation signal of 10mV, squares (■) to 50mV, rhombuses (♦) to 500mV and triangles (▲) to 1000mV.

Notice that points of extrema of one set of data (real or imaginary part) roughly coincide with the zeros of the other part, at the same frequency. Also note that the impedance data are almost unchanged when we vary the signal amplitude between 10 and 1000mV.

The fact that the spectra are independent of the applied signal amplitude indicates that the system is linear and no external noises sources are effective in determining the result of these measurements.

In spite of the proven linearity on the excitation signal, we also have constructed shields for the coil measurements. Four circuit shielding configurations for each coil were tested. Three of them used different kinds of aluminum shields and one setup was unshielded. One of the shields is cylindrical in shape, and possesses a length of 0.44m, an external diameter of 114mm and an internal diameter of 98mm. This geometry leads to a wall thickness of 8mm which is several times the skin dept of the radiation in aluminum at the lowest applied frequency (~0.8mm at 10KHz). The ends of this cylinder are also closed by two aluminum caps, 14mm thick, which are hermetically attached and screwed in the cylinder shield body. The coils are then inserted on this aluminum cylinder and centered along the cylinder axis with the aid of two stripes of insulation foam for support. With this configuration, a distance of 29mm is kept between the shield wall and the coil. Two BNC connectors are attached in the cylinder in order to make the coupling between the coils and the impedancemeter, and also to connect the shield to the impedancemeter ground. Pictures of this cylinder-shield are displayed on Figure 23.

Cylinder-shielded experiments

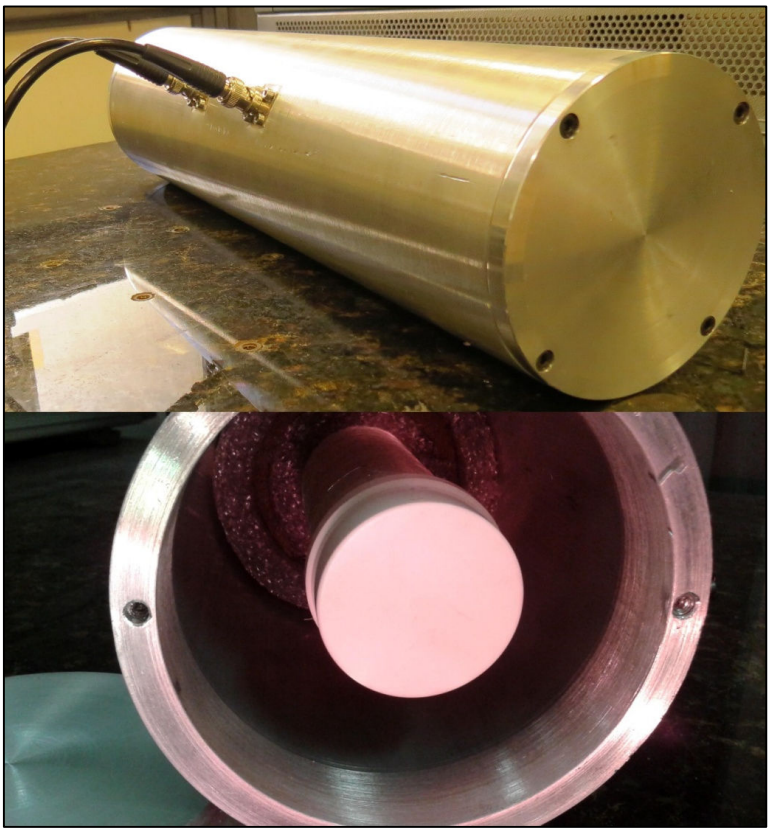

Figure 23: Pictures of the cylinder-shielded experiments. Top: closed shield connected to the impedancemeter. Bottom: side view of the open cylinder-shield displaying the enclosed coil.

Other shield configuration consisted of a rectangular box made with 5mm thick aluminum plates. The dimensions of this box are 0.80m x 0.45m x 0.45m. In this case the coils are also symmetrically placed, with their axis along the greater box dimension, held by insulating supports. These shield dimensions provide a distance from the shield walls to the coil of at least 0.20m. Two BNC connectors screwed on one side of this box provide electrical contacts to the impedancemeter through coaxial cables. Pictures of this box-shield are displayed on Figure 24.

Box-shielded experiments

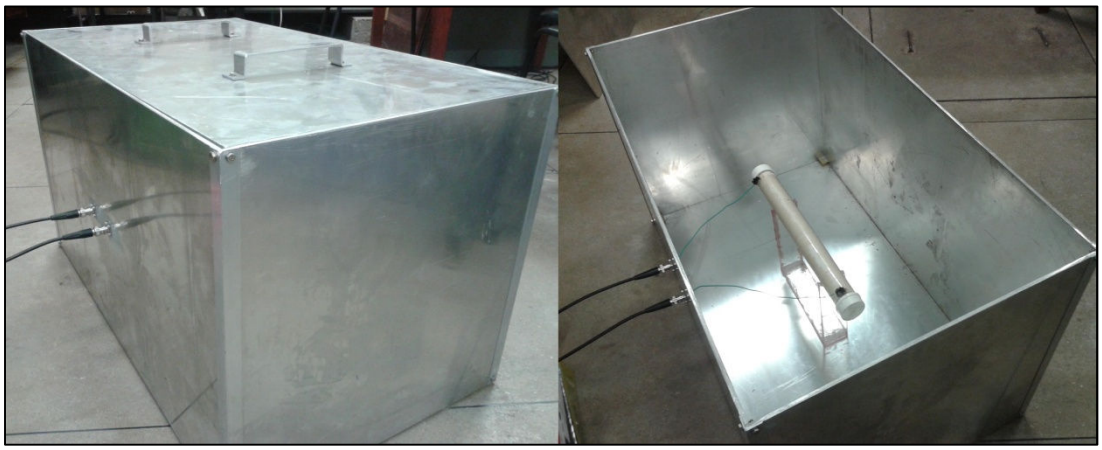

Figure 24: Pictures of the box-shielded experiments. Left: closed shield connected to the impedancemeter. Right: top view of the open box-shield displaying the enclosed coil.

The last shield type consisted of a 100μm thick aluminum foil, wrapped around the coils as tight as possible to its isolated wire. Pictures of this foil-shield, along with the unshielded coil are displayed on Figure 25.

Foil-shielded experiments

Figure 25: Foil-shielded experiments. Top: coil enclosed by the foil-shield. Bottom: unshielded coil.

Now we present raw data of the measurements for the different shielding configurations, performed on the constantan (constantan/27m/1.3mm/100μm) and the aluminum (Al/13m/1.4mm/10μm) coils. The resulting spectra for these experiments are plotted on Figure 26 (constantan) and on Figure 27 (aluminum).

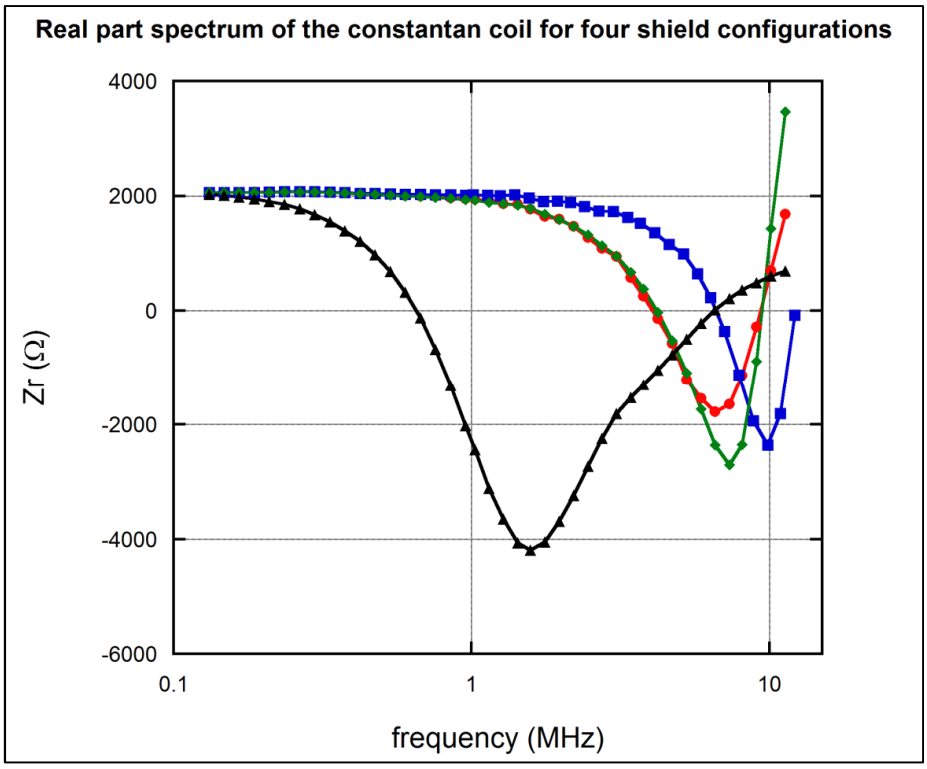

Figure 26: Real part spectrum of the constantan coil (constantan/27m/1.3mm/100µm) for four shield configurations. Circles (●) correspond to the unshielded coil, squares (■) to the box-shielded coil, rhombuses (♦) to the cylinder-shielded coil and triangles (▲) to the foil-shielded coil.

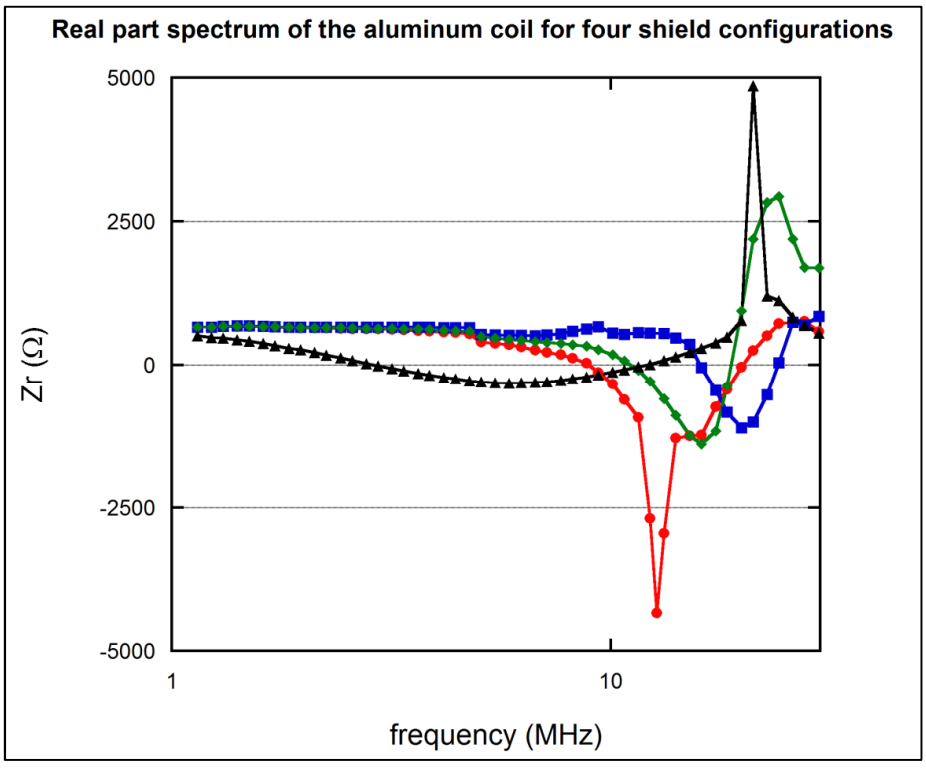

Figure 27: Real part spectrum of the aluminum coil (Al/13m/1.4mm/10µm) for four shield configurations. Circles (●) correspond to the unshielded coil, squares (■) to the box-shielded coil, rhombuses (♦) to the cylinder-shielded coil and triangles (▲) to the foil-shielded coil.

Each of these figures displays impedance data for four experimental configurations; the unshielded coil, the cylinder-shielded coil, the box-shielded coil and the foil-shielded coil. Regardless the way these shields disturb the spectra, the negative real part effect does not disappear in all cases. The fact that the negative real part impedance is observed with different kinds of coils, all them enclosed by shield walls several times thicker than the skin dept in the applied frequency, is a direct confirmation of this phenomenon. It excludes external sources as the cause for the observed effects. Since the negative real part peaks are dislodged to other frequency values sometimes lessened and sometimes augmented, we can conclude that wire near fields are important in causing this phenomenon. In particular we observed that the foil-shielded coils real parts become negative in lower frequency values when compared to the other experiments, changing its signal just below 1MHz for the constantan coil case.

4.5-Oscilloscope measurements

Qualitative measurements in the frequency range of 10 to 100MHz were also performed, using an external RF signal generator (Rohde & Schwarz - SMY01) and a 100MHz dual channel oscilloscope (Tektronix TDS 220) which has an input impedance of 1MΩ in parallel with a capacitance of 20pF. In this case, one channel reads the applied voltage in a coil and the other the voltage on a small value shunt resistor placed in series with the coil. This way, the voltage in the second channel is in-phase with the current in the circuit. This type of measurement generates less precise values for the impedance when compared to the impedancemeter but provides a direct comparison of voltage and current in the coil as function of time.

Measurements using an oscilloscope were performed on an unshielded coil. This experiment allows a direct view of the applied voltage and current in the circuit, if an in-series, pure resistive, small value shunt is used as a current sensor. Circuit current is in-phase with the voltage in the shunt in such a way that a direct comparison of voltage and current in the coil, as function of time, is possible. In order to achieve a good experimental condition a RF generator was plugged to a coil and the in-series 30Ω shunt. Channel 1 of the oscilloscope monitors the applied signal and channel 2 the voltage in the shunt. The scheme of this experimental setup is shown on Figure 28.

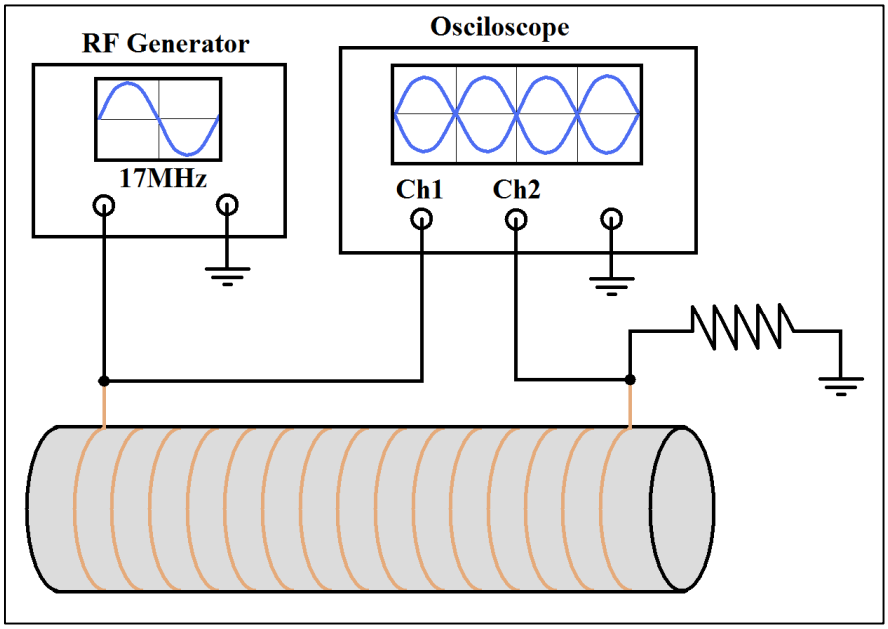

Figure 28: Experimental setup of the measurements made using an RF generator and an oscilloscope. They were performed at 17MHz and with a 30Ω shunt resistor in series with an aluminum coil.

Oscilloscope data for measurements made at 17MHz using an aluminum coil is shown on Figure 29.a.

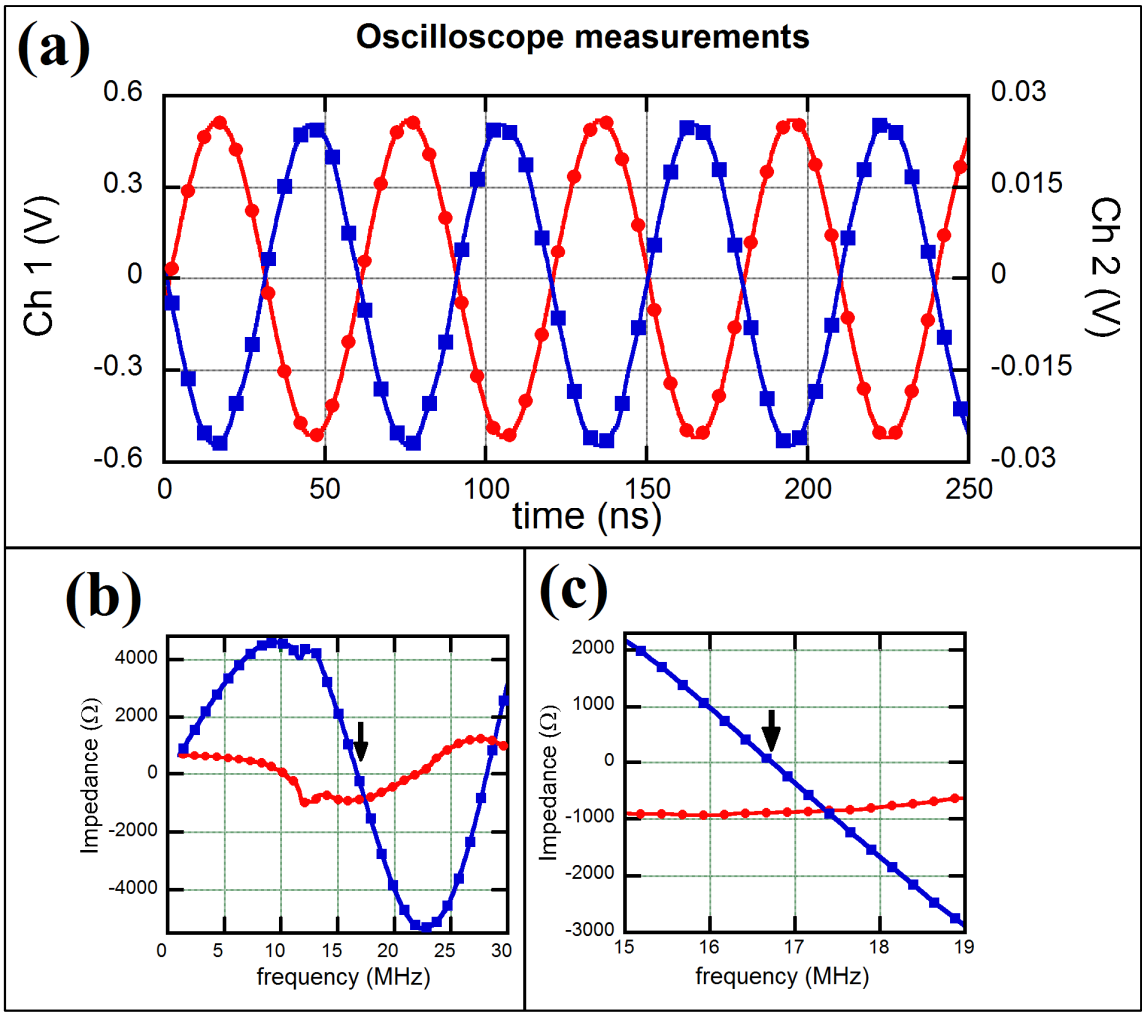

Figure 29: (a) Oscilloscope data of the measurements performed on an aluminum coil (Al/13m/1.4mm/10µm). On left vertical axis, circles (●) represent the Channel 1 voltage; on right vertical axis, squares (■) represent the Channel 2 voltage. (b) Impedance spectrum for this aluminum coil. Circles (●) represent the real part; and squares (■) represent the imaginary part. The arrow indicates a frequency, close to 17MHz, in which the imaginary part is zero and the real part is negative. (c) Detail of the spectrum of this coil in the vicinity of 17MHz.

Comparing both channels we can see a characteristic anti-phase picture, evidencing the negative real part impedance. Extreme anti-phasing, as shown here, suggests the existence of a frequency for which the negative real part coincides with a null imaginary part. This can be checked in Figure 29.b, where the spectrum of this coil is shown. For clearness, we present in Figure 29.c a detail of this spectrum. The arrow points to the zero of the imaginary part, which is very close to 17MHz. The imaginary part changes from positive (below ~17MHz) to negative values (above ~17MHz). It can be checked that, at this point, the real part in fact has a negative value. Thus the phase angle at this

frequency suffers a transition from π to $-\pi$, and leads to the anti-phase oscilloscope picture.

On an oscilloscope screen, visual confirmation of the anti-phase pattern in the 100 to 500MHz frequency range was also verified, with the use of a similar circuit configuration. A linear wire made of carbon fiber, having a length of 0.18m and in series with a 5mm length shunt made of the same material was used. Multiple inverted peaks were observed at various frequency values within this interval. This observation indicates that a device presenting negative resistance effects on tenths of meter scale could be feasible in the GHz region.

5-The negative real part impedance and causality issues

As discussed in the Introduction, negative real part impedances were not reported on linear passive circuits yet. In this work we have shown that electromagnetic field theory explains how the dynamics of the potentials produce this new impedance effect. Our model explicitly made use of retarded potentials so it is expected that causality is intrinsically satisfied. Still, a discussion on causality is pertinent on the grounds of the response theory.

There exist several means of checking impedance data for possible measurements errors. As result from Linear System Theory, the impedance functions must satisfy quite general conditions in order to make physical sense. First, the system is described by linear differential equations, so the principle of superposition must apply and the impedance values must be independent of the amplitude of the applied signal (linearity condition). Also, the system must be stable in time, in the sense that it returns to its original state after the perturbation is removed (stability condition). Another general condition that must be satisfied is that the impedance must be a continuous and finite valued function for all positive frequencies. Besides, any physically realizable impedance must be a causal function, that is, the system must not produce any response before the perturbation is applied and must not contain any other components from spurious sources (causality condition). These four conditions are the basis for the derivation of an integral transform commonly referred in the literature as Kramers-Kronig (K-K) relations. The K-K relations state that the real and the imaginary parts are not independent of each other, but related in a distinctive way, which outlines the causality condition. In fact, K-K equations are derived from a pair of Hilbert transformations, which constrain the real and negative parts of any truly causal transfer function, like the impedance. These relations were early applied to electrical networks [40] and to the analysis of electrochemical systems [57-60], after its logical foundations relating the causality and the origin of dispersion were made clear by Toll [61].

As discussed above, the impedance must be a linear, finite valued, stable in time and causal function. These issues were checked for our data. They are stable in time and signal amplitude independent (see Figure 22), meaning that our measurements represent linear impedances. Another necessary condition, fully checked, is that it is finite valued at all measured frequencies. Causality issues are more involved, since in this case, the real and imaginary parts must form a Hilbert Transform pair.

The logical foundations for causality were introduced by Toll [61], which made use of a theorem proved by Titchmarsh [62]. Toll explained, in a clear and rigorous way, in what sense a causal transfer function in time domain leads to a knowledge of its real and imaginary parts in the frequency domain. Specifically, in time domain the excitation signal (F_{in}) on a linear system is given by the convolution of a transfer function (T) and its response (F_{out}) as

$$F_{in}(t) = \int_{-\infty}^{\infty} F_{out}(u) T(t-u)\, du \tag{60}$$

Since the response cannot rise before the excitation, the transfer function must be causal, meaning that it is null for negative values of its argument. And for this same reason, we can also write the following equation:

$$T(t) = T(t)\Theta(t) \tag{61}$$

where Θ is the unit step function, that is, $\Theta = 1$ for $t > 0$ and $\Theta = 0$ for $t < 0$.
In our calculations, we follow Titchmarsh [62] and Toll [61], so the following definition of a direct Fourier transform is used:

$$\Im\{f(t)\} = \frac{1}{2\pi} \int_{-\infty}^{\infty} f(t) e^{i\omega t} dt \tag{62}$$

The impedance is defined as the Fourier transform of the transfer function as it was done on Equation 1. Given the causality condition demanded by Equation 61, the impedance is written as a convolution. Moreover this equation expresses a self-consistence relationship which must be satisfied by the impedance, and is given by

$$Z(\omega) = \Im\{T\Theta\} = \Im\{T\} * \Im\{\Theta\} = Z(\omega) * \Im\{\Theta\} \tag{63}$$

where the asterisk symbol denotes the convolution operation. The Fourier transform of the unit step distribution is calculated by use of Equation 62, and the result is

$$\Im(\Theta(t)) = \frac{1}{2}\delta(\omega) - \frac{1}{2\pi i\omega} \tag{64}$$

In consequence, an equation which must be satisfied by a causal function is obtained in the form:

$$Z(\omega) = -\frac{1}{\pi i\omega} * Z(\omega) \tag{65}$$

Equation 65 can be separated into its real and imaginary parts, and the result is the Hilbert transform pair [61, 63]:

$$\mathrm{Re}(Z(\omega)) = \frac{1}{\pi} P \int_{-\infty}^{\infty} \frac{\mathrm{Im}(Z(x))}{x-\omega} dx \tag{66}$$

$$\mathrm{Im}(Z(\omega)) = -\frac{1}{\pi} P \int_{-\infty}^{\infty} \frac{\mathrm{Re}(Z(x))}{x-\omega} dx \tag{67}$$

The letter P denotes the principal value of the improper integrals. Now we want to demonstrate that the impedance derived on Section 3.2 and represented by Equation 57 is a causal function, that is, it satisfies Equations 66 and 67. In order to achieve this goal, we firstly write down its real and imaginary parts explicitly as follows:

$$R(\omega) \equiv \mathrm{Re}\big(Z(\omega) - R\big) = \frac{-\omega\mu}{4\pi} \oint\oint \frac{\sin\big[\omega\big(s(\vec{r}\,') - |\vec{r} - \vec{r}\,'|\big)/c\big]}{|\vec{r} - \vec{r}\,'|} d\vec{s} d\vec{s}\,' \tag{68}$$

$$I(\omega) \equiv \mathrm{Im}\big(Z(\omega) - R\big) = \frac{\omega\mu}{4\pi} \oint\oint \frac{\cos\big[\omega\big(s(\vec{r}\,') - |\vec{r} - \vec{r}\,'|\big)/c\big]}{|\vec{r} - \vec{r}\,'|} d\vec{s} d\vec{s}\,' \tag{69}$$

The constant DC term was subtracted from theses equations. Notice that a Hilbert transform is a linear operator and commutes with both, the integral and derivative operators. Thus, when it is applied to the impedance expression displayed on Equation 57 (without the DC term) we must calculate the Hilbert transform of a function of the type $i\omega e^{i\omega q}$, that is, we have:

$$H\left\{i\omega e^{i\omega q}\right\} = \frac{d}{dq} H\left\{e^{i\omega q}\right\} = i\frac{d}{dq} e^{i\omega q} = -\omega e^{i\omega q} \tag{70}$$

After insertion of this result on Equation 57, we can expand the exponential and compare to Equations 68 and 69. This procedure readily leads to a pair of Hilbert transform for the real and imaginary parts and confirms the causality character of the impedance we have calculated. Explicitly the result is:

$$\mathrm{H}\big\{I(\omega)\big\} = \frac{1}{\pi} \int_{-\infty}^{\infty} \frac{I(x)}{x-\omega} dx = \mathrm{Re}(Z(\omega) - R) \tag{71}$$

$$-\mathrm{H}\big\{R(\omega)\big\} = \frac{-1}{\pi} \int_{-\infty}^{\infty} \frac{R(x)}{x-\omega} dx = \mathrm{Im}(Z(\omega) - R) \tag{72}$$

Shortly, the frequency-dependent term of the impedance displayed by Equation 57, generated by the space-dependent modulation on the current density, is causal, in complete consistence with the use of a retarded potential formula. As consequence, all requirements of the Linear System Theory are satisfied by our impedance data and calculations.

6-Conclusion and perspectives

After a brief historical review on the origins of impedance spectroscopy, we have summarized recent developments which represent several efforts to improve the accuracy and extend the limits of applicability of this technique, as well as to generate new applications and retrieve novel material properties.

Original results concerning the observation of a region of impedance spectra that was, until now unexploited, was presented in this work. The novelties presented here represent an advance towards a better understanding of the electrical impedance of a class of devices. They can be summarized as follows:

- Wave propagating modes for the current density: We have assumed the existence of propagating current waves inside an ohmic conductor. This hypothesis permitted us to devise a theoretical model which is in accordance with experimental results. This fact strongly favors our initial assumption as being realistic. Besides, experimental evidence concerning the direct observation of these waves was also provided.
- Prediction and measurements of novel impedances: Our model has predicted a region of the impedance spectrum which was never before observed. This prediction was confirmed by a set of careful executed experiments. The predicted and measured impedances have a negative real part. Equivalently, the impedance phase angle is capable of attaining a value of π. It was characterized by a new circuit element which complements the set comprising the standard set of R/L/C, and allows a full coverage of the trigonometric circle.
- Theoretical model for the electrodynamics of specific devices: By making use of the undulatory current assumption we were able to generate a theoretical model which permitted us to compute the dynamics of the electromagnetic potentials. As consequence, the electromagnetic fields and the impedance of a specifically designed device was obtained.
- Internal consistency: We have shown that, our modeling as well as our experimental data satisfies the criterions of Linear System Theory. In particular we have shown that the impedance we have obtained is a linear, finite valued, stable and causal function.

- Absence of mechanical analog: The obtained impedance presents no mechanical analog. This aspect is different in all the impedances already disseminated in the literature.

In as much as it occurred with the classical impedances of resistors, capacitors and inductors, the impedance described on this work may generate devices with a large extent of applicability. A patent including a class of devices which resulted from this work is pending. Some possible applications may be listed:

- Devices presenting negative real part impedance could be used in the construction a new class of oscillators which may be applied in a great variety of situations.
- Phase modulation, which is an important technique in telecommunications could greatly benefit from and extended phase element. That is because it encodes information as variations in the instantaneous phase of a carrier wave. So, an apparatus which could improve phase sensitivity would certainly permit the transmission of a greater amount of information.
- Matching impedance circuits are another class of devices which could be improved by use of negative real part impedances. The efficiency in the transmission of signals and/or power generally depends on impedance matching, which can be made easier with extended phase elements.

In regarding future perspectives, we may first cite a refinement on the theoretical modeling of the negative real part impedance effect. We have shown a calculation which presents the main features of the obtained experimental data, but an improvement in the agreement is certainly welcome. In order to improve the calculations some refinements can be made as to include the internal inductance contribution and the skin effect on the calculation of the extended phase impedance. Moreover, compact topology of spires and coils can be achieved in the GHz spectral region because much smaller wire length will be necessary to achieve a negative resistance component. This way, projects of circuits working in the extended phase region and designed for practical uses will become feasible. The physical system studied in this work presents essentially the same aspects of those studied by plasmonics, that is, the interaction of electromagnetic fields with the free electrons on conductors, in the infra-red range of frequencies. Thus, plasmonics may also be of relevance in the context of possible applications of the new phenomenology presented here.

References:

[1] J. Hicks et al. “A wide-bandgap metal-semiconductor-metal nanostructure made entirely from grapheme” Nature Physics vol. 9, pp. 49-54, 2012.

[2] K. Terabe, T. Hasegawa, T. Nakayama, and M. Aono, “Quantized conductance atomic switch” Nature vol. 433, pp. 47-50, 2005.

[3] D.B. Strukov, G.S. Snider, D.R. Stewart, and R.S. Williams, “The missing memristor found” Nature vol. 453, pp. 80-83, 2008.

[4] L.O. Chua, “Memristor - the missing circuit element” IEEE Trans. Circuit Theory vol. 18, pp. 507-519, 1971.

[5] P. Dutt, T.L. Schmidt, C. Mora, and K. Le Hur, “Strongly correlated dynamics in multichannel quantum RC circuits” Phys. Rev. B vol. 87, nº 155134, pp. 1-14, 2013.

[6] M. Buttiker, and S.E. Nigg, “ Mesoscopic capacitance oscillations” Nanotechnol. vol. 18, nº 044029, pp. 1-5, 2007.

[7] K. Inomata et al, “Microwave down-conversion with an impedance-matched Λ system in driven circuit QED” Phys. Rev. Lett. vol. 113, 063604, 2014.

[8] R. Waser, and M. Aono, “Nanoionics-based resistive switching memories” Nature Mater. vol. 6, pp. 833-840, 2007.

[9] N.B. Zhitenev, A. Sidorenko, D.M. Tennant, and R.A. Cirelli, “Chemical modification of the electronic conducting states in polymer nanodevices” Nature Nanotechnol. vol. 2, pp. 237-242, 2007.

[10] K. Szot, W. Speier, G. Bihlmayer, and R. Waser, “Switching the electrical resistance of individual dislocations in single-crystalline SrTiO3” Nature Mater. vol. 5, pp. 312-320, 2006.

[11] J.H.A. Smits, S.C.J. Meskers, R.A.J. Janssen, A.W. Marsman, and D.M. de Leeuw, “Electrically rewritable memory cells from poly(3-hexylthiophene) Schottky diodes” Adv. Mater. vol. 17, pp. 1169-1173, 2005.

[12] E. Warburg, “Uber das Verhalten Sogenannter Unpolarisierbarer Electroden Gegen Wechselstrom” Ann. Phys. Chem. vol. 67, pp. 493-499, 1899.

[13] I. Epelboin, M. Keddam and H. Takenouti, “Use of impedance measurements for the determination of the instant rate of metal corrosion” J. Appl. Electrochem. vol 2, pp. 71-79, 1972.

[14] D. Stepins, G. Asmanis and A. Asmanis, “Measuring capacitor parameters using vector network analyzers” Electronics vol. 18, pp. 29-38, 2014.

[15] Kuhn W. B and Boutz A. P, “Measuring and reporting high quality factors of inductors using vector network analyzers”, IEEE T. Microw. Theory vol. 58, pp. 1046-1055, 2010.

[16] Y. Tagro et. al, “In situ silicon-integrated tuner for automated on-wafer MMW noise parameters extraction using multi-impedance method for transistor characterization” IEEE T. Semiconduct. M. vol. 25, pp. 170-177, 2012.

[17] J. Liu, U. Frühauf, and A. Schönecker “Accuracy improvement of impedance measurements by using the self-calibration” Measurement vol. 25, pp. 213-225, 1999.

[18] J. Liu and U. Frühauf , “Self-calibration measuring methods and applications to measurements of electrical quantities” Measurement vol. 26, pp. 129-142, 1999.

[19] L. Angrisani and L. Ferrigno, “Reducing the uncertainty in real-time impedance measurements” Measurement vol. 30, pp. 307-315, 2001.

[20] L. Navarro, E. Mayevskiy and T. Chairet, “Measurements of characteristic impedance of high frequency cables with Time Domain Reflectometry TDR” ARFTG Microwave Measurement Symposium, 72nd, IEEE, Portland 2008.

[21] P. C. Gregory, “Impedance measurements of a loop antenna in the topside ionosphere” Planet. Space Sci. vol. 18, pp. 1357-1365, 1970.

[22] M. Tsutsui et al. “Measurements and analysis of antenna impedance aboard the Geotail spacecraft” Radio Sci. vol. 32, pp. 1101-1126, 1997.

[23] H. Zhu, Y. C. A. Ko and T. T. Ye, “Impedance measurement for balanced UHF RFID tag antennas” Radio and Wireless Symposium (RWS), IEEE, New Orleans, 2010.

[24] M. Gebhart, T. Baier and M. Facchini, “Automated antenna impedance adjustment for near field communication (NFC)” 12th International Conference on Telecommunications – ConTEL, Zagreb 2013.

[25] M. Randus and K. Hoffmann, “A novel method for direct impedance measurement in microwave and mm-wave bands” Microwave Measurements Conference, 75th ARFTG, IEEE, Anaheim 2010.

[26] T. Okada et al. “Microwave surface-impedance measurements of the electronic state and dissipation of magnetic vortices in superconducting LiFeAs single crystals” Phys. Rev. B vol. 86, 064516, 2012.

[27] J. D. Kim et al. “Impedance measurement system for a microwave-induced plasma” J. Korean. Phys. Soc. vol. 60, pp. 907-911, 2012.

[28] R. Swarup, P. S. Negi and R. L. Mendiratta, “Estimation of uncertainty in impedance measurement at narrow and broadband microwave frequencies” Measurement vol. 33, pp. 55-66, 2003.

[29] L. Callegaro, “The metrology of electrical impedance at high frequency: a review” Meas. Sci. Technol. vol. 20, 022002, 2009.

[30] P. Ferloni, M. Mastragostino and L. Meneghello, “Impedance analysis of electronically conducting polymers” Electrochim. Acta vol. 41, pp. 27-33, 1996.

[31] R. B. Sardenberg, C. E. Teixeira, M. Pinheiro, and J. M. A. Figueiredo, “Nonlinear conductivity of fullerenol aqueous solutions” ACS Nano vol. 5, pp. 2681-2686, 2011.

[32] T. A. Nguyen, Tsung-I. Yin, D. Reyes, and G. A. Urban, “Microfluidic Chip with Integrated Electrical Cell-Impedance Sensing for Monitoring Single Cancer Cell Migration in Three-Dimensional Matrixes” Anal. Chem. vol. 85, pp. 11068-11076, 2013.

[33] F. A. Atienzar, H. Gerets, K. Tilmant, G. Toussaint, and S. Dhalluin, “Evaluation of Impedance-Based Label-Free Technology as a Tool for Pharmacology and Toxicology Investigations”. Biosensors vol. 3, pp. 132-156, 2013.

[34] F. Huet, “A review of impedance measurements for determination of the state-of-charge or state-of-heath of secondary batteries” J. Power Sources vol. 70, pp.59-69, 1998.

[35] G. Gramse, “Calibrated complex impedance and permittivity measurements with scanning microwave microscopy” Nanotechnology vol. 25, 145703, 2014.

[36] G. Maurin, O. Solorza and H. Takenouti, “CdTe electrodeposition some new data from AC impedance” J. Electroanal. Chem. vol. 202, pp. 323-328, 1986.

[37] S. Rouquette-Sanchez, P. Cowache, P. Boncorps and J. Vedel, “Theoretical investigation of the electrochemical deposition of metal involving adsoption and desorption steps” Electrochim. Acta vol. 38, pp. 2043-2050, 1993.

[38] G. Salié, “Oscillatory kinetics of electrochemical phase boundary reactions” J. Electroanal. Chem. vol. 116, pp. 625-642, 1980.

[39] V. I. Shnyrkov, D. Born, A. A. Soroka, and W. Krech, “Coherent Rabi response of a charge-phase qubit under microwave irradiation” Phys. Rev. B vol. 79, 184522, 2009.

[40] H. W. Bode, “Network analysis and feedback amplifier design” Bell telephone laboratories series, D. Van Nostrand Company, Inc. New York 1945.

[41] J. Kowal, D. Hente and D. Sauer, “Model parameterization of nonlinear devices using impedance spectroscopy” IEEE T. Instrum. Meas. vol. 58, pp. 2343-2350, 2009.

[42] Quadrature Signals: Complex, But not Complicated, by Richard Lyons. Available at: http://www.ieee.li/pdf/essay/quadrature_signals.pdf

[43] Agilent Impedance Measurement Handbook – A guide to measurement technology and techniques 4th Edition. Available at: http://www.keysight.com/

[44] J. C. Shedd and M. D. Hersey, "The history of Ohm's law" Popular Science Monthly, vol. 83 pp. 599-614 1913.

[45] N. W. Ashcroft and D. N. Mermin, "Solid State Physics" Harcourt College Publishers, pp. 2-11, New York, 1976.

[46] J. Roche, "Explaining electromagnetic induction: a critical re-examination" Phys. Educ., vol. 22 pp. 91-99 1987.

[47] A. Mills, "Studies in electrostatics – Part 6: The Leyden Jar and other capacitors" Bulletin of the Scientific Instrument Society vol. 99, pp. 20-22 2008.

[48] S. Luryi, "Quantum capacitance devices" Appl. Phys. Lett. vol. 52, pp. 501-503 1988.

[49] Z. L. Mišković and N. Upadhyaya, "Modeling electrolytically top-gated graphene" Nanoscale Res. Lett. vol. 5 pp. 505-511 2010.

[50] A. S. Everest, "Kirchhoff-Gustav Robert 1824-1887" Phys. Educ. vol. 4 pp. 341-343 1969.

[51] A. Fick, "On liquid diffusion" Journal of Membrane Science vol. 100, pp. 33-38 1995.

[52] A. Einstein, "Über die von der molekularkinetischen Theorie der Wärme geforderte Bewegung von in ruhenden Flüssigkeiten suspendierten Teilchen" Annalen der Physik vol. 322 (8) pp. 549-560 1905.

[53] R. Sardenberg and J. M. A. Figueiredo, "Relationship between spatial and spectral properties of ionic solutions: The distributed impedance of an electrolytic cell" Electrochimica Acta, vol. 55, pp. 4722-4727 2010.

[54] J. D. Jackson, "Classical Electrodynamics" John Wiley & Sons; 1999.

[55] S. Ramo, J. R. Whinnery, T. Van Duzer, "Fields and waves in communication electronics" 3rd ed. New York (NY): John Wiley & Sons; 1994.

[56] Alpha-A High Resolution Dielectric, Conductivity, Impedance and Gain Phase Modular Measurement System, User's Manual, Issue: 5/2009 Rev. 2.9 by Novocontrol Technologies GmbH & Co. KG.

[57] D. D. Macdonald and M. Urquidi-Macdonald, “Application of Kramers-Kronig transforms in the analysis of electrochemical systems: I Polarization resistance” J. Electrochem. Soc. vol. 132, pp. 2316-2319, 1985.

[58] M. Urquidi-Macdonald, S. Real and D. D. Macdonald, “Application of Kramers-Kronig transforms in the analysis of electrochemical impedance data: II Transformations in the complex plane” J. Electrochem. Soc. vol. 133, pp. 2018-2024, 1986.

[59] J. M. Esteban and M. E. Orazem, “On the application of the Kramers-Kronig relations to evaluate the consistency of electrochemical impedance data” J. Electrochem. Soc. vol. 138, pp. 67-76, 1991.

[60] B. A. Boukamp, “Practical application of the Kramers-Kronig transformation on impedance measurements in solid state electrochemistry” Solid State Ionics vol. 62, pp. 131-141, 1993.

[61] J. S. Toll, “Causality and the dispersion relation: logical foundations” Phys. Rev. vol. 104, pp. 1760-1770, 1956.

[62] E. C. Titchmarsh, “Introduction to the theory of Fourier Integrals”, Clarendon Press, Oxford, 2nd ed. pp. 119-128, 1948.

[63] R. N. Bracewell, “The Fourier transform and its applications”, McGraw-Hill, 3rd ed. pp. 359-364, 2000.